

1 **Long-term incubations provide insight into the mechanisms of anaerobic**
2 **oxidation of methane in methanogenic lake sediments**

3 Hanni Vigderovich^a, Werner Eckert^b, Michal Elul^a, Maxim Rubin-Blum^c, Marcus Elvert^d, Orit Sivan^a

4 ^aDepartment of Earth and Environmental Science, Ben-Gurion University of the Negev, Beer Sheva, Israel

5 ^bIsrael Oceanographic & Limnological Research, The Yigal Allon Kinneret Limnological Laboratory, Israel

6 ^cIsrael Oceanographic & Limnological Research, Haifa, Israel

7 ^dMARUM - Center for Marine Environmental Sciences and Faculty of Geosciences, University of Bremen,
8 Bremen, Germany

9 *Corresponding author:* Hanni Vigderovich, hannil@post.bgu.ac.il

10 **Abstract**

11 Anaerobic oxidation of methane (AOM) is among the main processes limiting the release of the
12 greenhouse gas methane from natural environments. Geochemical profiles and experiments with fresh
13 sediments from Lake Kinneret (Israel) indicate that iron-coupled AOM (Fe-AOM) sequesters 10-15%
14 of the methane produced in the methanogenic zone (> 20-cm sediment depth). The oxidation of methane
15 in this environment was shown to be mediated by a combination of *mcr* gene-bearing archaea and *pmoA*
16 gene-bearing aerobic bacterial methanotrophs. Here, we used sediment slurry incubations under
17 controlled conditions to elucidate the electron acceptors and microorganisms that are involved in the
18 AOM process over long-term (~18 months). We monitored the process with the addition of ¹³C-labeled
19 methane and two stages of incubations: (i) enrichment of the microbial population involved in AOM
20 and (ii) slurry dilution and manipulations, including the addition of several electron acceptors (metal
21 oxides, nitrate, nitrite and humic substances) and inhibitors (2-bromoethanesulfonate, acetylene and
22 sodium molybdate) of methanogenesis, methanotrophy and sulfate reduction/sulfur disproportionation.
23 Carbon isotope measurements in the dissolved inorganic carbon pool suggest the persistence of AOM,
24 consuming 3-8% of the methane produced at a rate of 2.0±0.4 nmol g⁻¹ dry sediment day⁻¹. Lipid carbon
25 isotopes and metagenomic analyses point towards methanogens as the sole microbes performing the
26 AOM process by reverse methanogenesis. Humic substances and iron oxides, but not sulfate,
27 manganese, nitrate, or nitrite, are the likely electron acceptors used for this AOM. Our observations
28 support the contrast between methane oxidation mechanisms in naturally anoxic lake sediments, with
29 potentially co-existing aerobes and anaerobes, and long-term incubations, wherein anaerobes prevail.

30

31 Keywords: Anaerobic oxidation of methane (AOM), lake sediments, dissolved inorganic carbon, stable
32 carbon isotopes, electron acceptors, archaea, methanogens, methanotrophs, lipids.

33

34 **1. Introduction**

35 Methane (CH₄) is an important greenhouse gas (Wuebbles and Hayhoe, 2002), which has both
36 anthropogenic and natural sources, the latter of which account for about 50% of the emission of this gas
37 to the atmosphere (Saunio et al., 2020). Naturally occurring methane is mainly produced biogenically
38 via the methanogenesis process, which is performed by methanogenic archaea. Traditionally
39 acknowledged as the terminal process anchoring carbon remineralization (Froelich et al. 1979),
40 methanogenesis occurs primarily via the reduction of carbon dioxide by hydrogen in marine sediments
41 and via acetate fermentation in freshwater systems (Whiticar et al. 1986).

42 Methanotrophy, the aerobic and anaerobic oxidation of methane (AOM) by microbes, naturally controls
43 the release of this gas to the atmosphere (Conrad, 2009; Reeburgh, 2007; Knittel and Boetius, 2009). In
44 marine sediments, up to 90% of the upward methane flux is consumed anaerobically by sulfate, and in
45 established diffusive profiles, that methane consumption occurs within a distinct sulfate-methane
46 transition zone (Valentine 2002). While sulfate-dependent AOM, catalyzed by the archaeal ANaerobic
47 MEthanotrophs (ANMEs) 1-3, is widespread chiefly in marine sediments (Hoehler et al., 1994; Boetius
48 et al., 2000; Orphan et al., 2001; Treude et al., 2005, 2014), methane oxidation in other environments
49 can be coupled to other electron acceptors (e.g. Raghoebarsing et al., 2006; Ettwig et al. 2010; Sivan et
50 al., 2011; Crowe et al. 2011; Norði and Thamdrup 2014; Valenzuela et al., 2017).

51 In freshwater sediments sulfate is often depleted, and methanogenesis may be responsible for most of
52 the organic carbon remineralization, resulting in thus high concentrations of methane in shallow
53 sediments (Sinke et al., 1992). Indeed, lakes and wetlands, are responsible for 33-55% of naturally
54 emitted methane (Rosentreter et al., 2021). A large portion of this produced methane is oxidized by
55 aerobic (type I) methanotrophic bacteria via oxygen. Aerobic methanotrophy is generally observed in
56 the sediment-water interface (Damgaard et al. 1998) and/or in the water column thermocline (Bastviken
57 2009). AOM, however, can also consume over 50% of the produced methane (Segarra et al. 2015).

58 Sulfate can be an electron acceptor of AOM in freshwater sediments, as was shown for example in Lake
59 Cadagno (Schubert et al., 2011, Su et al., 2020). Alternative electron acceptors for AOM in natural
60 freshwater environments and cultures include humic substances, nitrate, nitrite and metals (such as iron
61 manganese and chromium). Natural humic substances and their synthetic analogs were shown to
62 function as terminal electron acceptors for AOM in soils, wetlands and cultures (Valenzuela et al., 2017;
63 2019; Bai et al., 2019; Zhang et al., 2019; Fan et al., 2020). Nitrate-dependent AOM has been
64 demonstrated in a consortium of archaea and denitrifying bacteria from a canal (Raghoebarsing et al.,
65 2006), in freshwater lake sediments (Norði and Thamdrup 2014) and in a sewage enrichment culture of
66 ANME-2d (Haroon et al., 2013; Arshad et al., 2015). Nitrite is exploited to oxidize methane by the
67 aerobic bacteria *Methyloirabilis* (NC-10), which split the nitrite to N₂ and O₂ and then uses the

68 produced oxygen to oxidize the methane (Ettwig et al., 2010). ANME-2d were also suggested to be
69 involved in Cr(VI) coupled AOM, either alone or with a bacterial partner (Lu et al., 2016). Iron and/or
70 manganese coupled AOM have also been suggested in lakes (Sivan et al., 2011; Crowe et al. 2011;
71 Norđi et al., 2013), sometimes by supporting sulfate-coupled AOM (Shubert et al., 2011; Su et al., 2020;
72 Mostovaya et al., 2021). Iron-coupled AOM was also shown to occur in enriched, denitrifying cultures
73 from sewage where it was performed by ANME-2 (Ettwig et al. 2016), and in a bioreactor with natural
74 sediments (Cai et al., 2018).

75 The mechanism and role of iron-coupled AOM in lake sediments have been studied with a variety of
76 tools in the sediments of Lake Kinneret. *In-situ* pore water profiles and top core experiments (Sivan et
77 al., 2011), diagenetic models (Adler et al., 2011) and batch incubation experiments with fresh sediment
78 slurries (Bar-Or et al., 2017) suggest that iron coupled-AOM (Fe-AOM) removes 10-15% of the
79 produced methane in the deep methanogenic zone (> 20 cm below the water-sediment interface).
80 Analysis of the microbial community structure suggested that both methanogenic archaea and
81 methanotrophic bacteria are potentially involved in methane oxidation (Bar-Or et al., 2015). Analyses
82 of stable isotopes in fatty acids, 16S rRNA gene amplicons and metagenomics showed that both reverse
83 methanogenesis by archaea and bacterial type I aerobic methanotrophy by Methylococcales play
84 important role in methane cycling (Bar-Or et al., 2017; Elul et al., 2021). Aerobic methanotrophy, which
85 has also been observed in the hypolimnion and sediments of several other lakes that are considered
86 anoxic (Beck et al., 2013; Oswald et al., 2016; Martinez-Cruz et al., 2017; Cabrol et al., 2020), may be
87 driven by the presence of oxygen at nanomolar levels (Weng et al., 2018). Pure cultures of the
88 ubiquitous aerobic methanotrophs Methylococcales have indeed been shown to survive under hypoxia
89 either by oxidizing methane and with nitrate (Kits et al., 2015), by switching to iron reduction (Zheng
90 et al., 2020), or even by exploiting their methanobactins to generate their own oxygen to fuel their
91 methanotrophic activity (Dershwitz et al., 2021). The latter study also showed that the
92 alphaproteobacterial methanotroph *Methylocystis* sp., strain SB2, can couple methane oxidation and
93 iron reduction. However, whether these aerobic methanotrophic bacteria are able to oxidize methane
94 under strictly anoxic conditions and which electron acceptors are available to facilitate that activity are
95 still not known.

96 In the current study, we used long-term anaerobic incubations to assess the dynamics of methane-
97 oxidizing microbes under anoxic conditions and to quantify the respective availabilities of different
98 electron acceptors for AOM. To that end, we diluted fresh methanogenic sediments from Lake Kinneret
99 with original porewater from the same depth and amended the sediment with ¹³C-labeled methane. Our
100 experiment design comprised two stages, the first of which included the enrichment of the microbial
101 population involved in AOM, while the second involved an additional slurry dilution and several
102 manipulations with different electron acceptors and inhibitors. We measured methane oxidation rates
103 (based on ¹³C-DIC enrichment), determined the characteristics of each electron acceptor (via its

104 turnover), and evaluated changes in microbial diversity over various incubation periods (based on
105 metagenomics and lipid biomarkers). The results from the long-term anaerobic incubations were
106 compared to those of batch and semi-continuous bioreactor experiments.

107 **2. Methods**

108 **2.1 Study site**

109 Lake Kinneret (Sea of Galilee) is a warm, monomictic, freshwater lake that is 21 km long and 13 km
110 wide and located in northern Israel. Its maximum depth is ~42 m at its center (station A, Figure S1)
111 while its average depth is 24 m. From March to December, the lake is thermally stratified, and from
112 April to December, the hypolimnion is anoxic. Surface water temperatures range from 15°C in the
113 winter (January) to 32°C in the summer (August), while the lake's bottom water temperatures remain
114 in the range of 14-17°C throughout the year. The sediment from the deep methanogenic zone used in
115 this study (sediment samples taken from a sediment depth of ~20 cm from the water-sediment interface
116 at the lake's center) contains 50% carbonates, 30% clay and 7% iron (Table S1). The dissolved organic
117 carbon (DOC) concentration of the porewater increases with depth, ranging from ~6 mg C L⁻¹ at the
118 sediment-water interface to 17 mg C L⁻¹ at a depth of 25 cm (Adler et al., 2011). The concentrations of
119 dissolved methane in the sediment porewater increase sharply with sediment depth, reaching a
120 maximum of more than 2 mM at a depth of 15 cm, after which the amounts of dissolved methane
121 gradually decreased with depth to 0.5 mM at a depth of 30 cm (Adler et al., 2011; Sivan et al., 2011;
122 Bar-Or et al., 2015).

123 **2.2 Experimental setup**

124 2.2.1 General

125 In this study we compared three incubation strategies (A, B and C; Fig. 1) in Lake Kinneret
126 methanogenic sediments (sediment depths > 20 cm), which were amended with original porewater from
127 the same depth, ¹³C-labeled methane, different potential electron acceptors for AOM (nitrite, nitrate,
128 iron and manganese oxides and humic substances) and activity inhibitors. We inhibited the *mcr* gene
129 with 2-bromoethanesulfonate (BES), methanogenesis and methanotrophy with acetylene, and sulfate
130 reduction and sulfur disproportionation with Na-Molybdate (Nollet et al., 1997; Oremland & Capone,
131 1988; Lovley & Klug, 1983). Below we describe the three incubation strategies (Fig. 1).

132 A) Long-term, two-stage slurry incubations with a 1:1 sediment to porewater ratio and high methane
133 content for the first three months (first stage) to ensure the enrichment of the microorganisms involved
134 in AOM. After three months, the slurry was diluted with porewater to a 1:3 ratio (second stage) and
135 different reactants were added to the incubations, which were subsequently monitored for up to 18
136 months.

137 B) Semi-continuous bioreactor experiments in which sediments were collected up to three days before
138 the experiment was set up (freshly sampled sediments) and sediment to porewater ratio of 1:4, where
139 porewater was exchanged regularly.

140 C) Batch incubation experiments with freshly sampled sediments and porewater at a 1:5 ratio,
141 respectively, and amended with hematite. This experimental set-up was described in our previous
142 studies (Bar-Or et al., 2017; Elul et al., 2021).

143 The sediments for the slurries conducted in the current work were collected during seven sampling
144 campaigns aboard the research vessel *Lillian* between 2017 and 2019 from the center of the lake (Station
145 A, Fig. S1) using a gravity corer with a 50-cm Perspex core liner. The length of the sediment in each
146 core was 35-45 cm. During each sampling campaign, 1-2 sediment cores were collected for the
147 incubations and 10 cores were collected for the porewater extraction. Sediments from the methanogenic
148 zone (sediment depths > 20 cm) were diluted with porewater from the methanogenic zone of parallel
149 cores sampled on the same day. The porewater was extracted on the day of sampling. The sediment
150 cores were sliced while onboard, and sediment samples from the methanogenic zone (> 20 cm) were
151 transferred to a dedicated container. In the lab, sediments were collected with 20-ml cutoff syringes and
152 moved to 50-ml falcon tubes. The porewater was extracted by centrifugation at 9300 g for 15 min at
153 4°C, filtered by 0.22-µm filters into 250-ml pre-autoclaved glass bottles, crimp-sealed with rubber
154 stoppers, and flushed for 30 min with N₂. The extracted porewater was kept under anaerobic conditions
155 at 4 until its use. The sediments for the incubations were subsamples from the liners and diluted no later
156 than three days after their collection from the lake and treated further according to the experimental
157 strategies described above (setup A or B).

158 2.2.2 Experiment type A set-up: Long-term two-stage incubations (henceforth referred to as “two-
159 stage” for simplicity)

160 Experiment A comprised ten two-stage incubation experiments (experiment serial numbers (SN) 1-10;
161 Table 1) with different treatments (electron acceptors/shuttling/inhibitors). In the first stage (pre-
162 incubation slurry), the sediment core was sliced under a N₂ atmosphere and sediments from depths > 20
163 cm were collected into zipper bags. The sediment was homogenized, and between 80-100 gr transferred
164 into 250-ml glass bottles under continuous N₂ flushing. The sediments were diluted with the extracted
165 porewater to create a 1:1 sediment to porewater slurry with a headspace of 70-90 ml (Fig. 1). The
166 slurries were sealed with rubber stoppers and crimped caps and were flushed with N₂ (99.999%,
167 MAXIMA, Israel) for 30 min. Methane (99.99%, MAXIMA, Israel) was injected using a gas-tight
168 syringe for a final content of 20% in the headspace, where 10% of the injected methane was ¹³C-labeled
169 methane (99%, Sigma-Aldrich). When significant AOM activity was observed based on the increase of
170 δ¹³C_{DIC} after approximately three months (Fig. S2), some of the incubations were further diluted during

171 the second stage of the experiments. The remainder of the incubations continued to be run with
172 porewater exchange while the $\delta^{13}\text{C}_{\text{DIC}}$ values were monitored every three months.

173 All the experiments were set up similarly (see dates and detailed protocols in the supplementary
174 information): the pre-incubation bottle was opened and subsamples (~18 g each) were transferred with
175 a syringe and a Tygon® tube under a laminar hood and continuous flushing of N_2 gas into 60-ml glass
176 bottles. The subsamples were then diluted with fresh anoxic porewater from the methanogenic zone (as
177 described above) to achieve a 1:3 sediment to porewater ratio (Fig. 1) while leaving 24 ml of headspace
178 in each bottle. The bottles were crimp-sealed, flushed with N_2 gas for 5 min, shaken vigorously and
179 flushed again (3 times). Then ^{13}C -labeled methane was added to all of the bottles as described in Table
180 1. The "killed" control slurries in each experiment were autoclaved twice and cooled, only after which
181 they were amended with the appropriate treatments and ^{13}C -labeled methane.

182 To the diluted (1:3) batch slurries electron acceptors were added either as a powder (hematite –
183 experiment no. 1, magnetite – experiment no. 2, clay and humic substances – experiment no. 7, MnO_2
184 – experiment no. 3) or in dissolved form in double-distilled water (DDW) (KNO_3 – experiment no. 4,
185 NaNO_2 – experiment no. 5). In addition, the potential involvement of sulfur cycling in the transfer of
186 electrons was tested in experiment no. 2 via its inhibition with Na-molybdate (Lovley and Klug, 1983).
187 The synthetic analog for humic substances, i.e., 9,10-anthraquinone-2,6-disulfonate (AQDS), was
188 dissolved in DDW (detailed in the supplementary information) and added to the bottles of experiment
189 no. 6 until a final concentration of 5 mM was achieved in each bottle. Amorphous iron ($\text{Fe}(\text{OH})_3$) was
190 prepared in the lab by dissolving FeCl_3 in DDW that was then titrated with NaOH 1.5 N up to pH 7 and
191 injected to the bottles of experiment no. 2. The final concentration of each addition is detailed in Table
192 1. The ^{13}C -labeled methane was injected into all of the experimental bottles at the beginning of each
193 experiment (unless described otherwise) by using a gas-tight syringe from a stock bottle filled with ^{13}C -
194 labeled methane gas (which was replaced with saturated NaCl solution). Three different inhibitors were
195 added to three different experiments: Molybdate was added to experiment No. 1 (to one bottle of
196 methane-only treatment, magnetite treatment and amorphous iron treatment) to detect the feasibility of
197 an active sulfur cycle; BES was added to experiment No. 8 at the start of the experiment; and acetylene
198 was added to experiment No. 9, wherein it was injected during the experiment into two bottles at
199 different timepoints after ^{13}C enrichment was observed in the DIC (Table 1).

200 All live treatments were set up in duplicate or triplicate, depending on the amount of the pre-incubated
201 slurry aimed for each experiment, and the results are presented as the average with an error bar. In two
202 experiments, only one "killed" control bottle was set up, and the remainder of the slurry was prioritized
203 for other treatments, because the killed controls repeatedly showed no activity in several previous
204 experiments. The humic substrate experiment used a natural (humic) substance that was extracted from
205 a lake near Fairbanks, Alaska, where the iron reduction was observed in the methanogenic zone. One

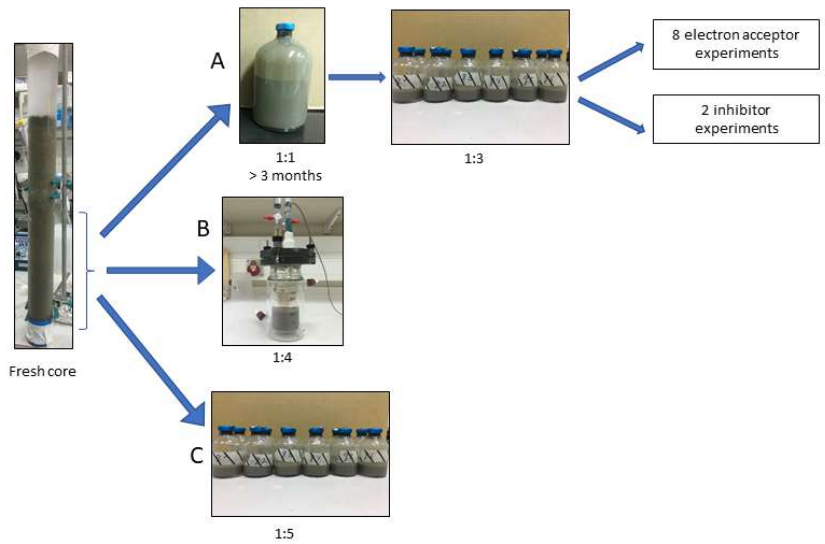
206 experiment was set up without any additional electron acceptor to assess the rate of methanogenesis in
207 the two-stage slurries. Porewater was sampled anaerobically for $\delta^{13}\text{C}_{\text{DIC}}$ and dissolved Fe(II)
208 measurements in duplicate (2 ml), and methane was measured from the headspace. Variations in the
209 $\delta^{13}\text{C}_{\text{DIC}}$ values between the experiments resulted from different amounts of ^{13}C -labeled methane injected
210 at the start of each experiment (geochemical measurements detailed in the analytical methods section
211 below).

212 2.2.3 Experiment type B setup: Semi-continuous bioreactor

213 Semi-continuous bioreactors were used to monitor the redox state regularly at close-to-natural *in-situ*
214 conditions for 15 months in freshly collected sediments. Two 0.5-L semi-continuous bioreactors (Fig.
215 1) (LENZ, Weinheim, Germany) were set up with freshly sampled sediments from the methanogenic
216 zone (25 - 40 cm) and extracted porewater from the same depth from Station A on Lake Kinneret
217 immediately after their collection. Both reactors were filled, headspace-free, with a slurry at a 1:4
218 sediment to porewater ratio. One bioreactor was amended with 10 mM hematite while the second, which
219 was a control, was not amended. To dissolve ^{13}C -labeled methane in the porewater, 15 ml of porewater
220 were replaced with 15 ml of methane gas (13 ml of $^{12}\text{CH}_4$ and 2 ml of $^{13}\text{CH}_4$) to produce a methane-
221 only headspace for 24 h, during which time the reactors were shaken repeatedly. After 24 h, the gas was
222 replaced with anoxic porewater, thus eliminating the headspace, which resulted in lower methane
223 concentrations (0.2 mM) than in either the two-stage incubations or the fresh batch experiment (~2 m).
224 The redox potential was monitored continuously using a platinum/glass electrode (Metrohm, Herisau,
225 Switzerland) to verify anoxic conditions and to determine the redox state throughout the incubation
226 period. The bioreactors were subsampled weekly to bi-weekly, and the sample volume (5-10 ml) was
227 replaced immediately by preconditioned anoxic (flushed with N_2 gas for 15 min) porewater from the
228 methanogenic zone. As outlined below, samples were analyzed for dissolved Fe(II), methane and
229 $\delta^{13}\text{C}_{\text{DIC}}$. Additional subsamples for metagenome and lipid analyses were taken at the beginning of the
230 experiment and on days 151 and 382, respectively.

231 2.2.4 Experiment type C setup: Fresh batch experiment

232 Sediments for this experiment were collected in August 2013 at Station A using a protocol similar to
233 that used to collect the sediments for the pre-incubations. Sediments from depths greater than 26 cm
234 were diluted under anaerobic conditions with porewater from the same depth to obtain a ratio of
235 sediment to porewater of 1:5. The resulting slurry was then divided between 60-ml glass bottles (40 ml
236 slurry in each bottle). The sampling and experimental setup are described in detail in our earlier study
237 (Bar-Or et al., 2017). Here we present our results of the $\delta^{13}\text{C}_{\text{DIC}}$, metagenome and lipid analyses of two
238 treatments: natural (with only ^{13}C -labeled methane) and hematite. The experiment ran for 15 months.



239

240 Figure 1: Flow diagram of the experimental design. Three types of experiments were set up to investigate the
 241 methanogenic zone sediments (deeper than 20 cm): **A)** Two-stage slurry experiments, with 1:1 ratio of sediment
 242 to porewater incubations and then with diluted pre-incubated slurries and porewater (1:3 ratio of sediment to
 243 porewater). **B)** Semi-aerobic bioreactor experiment with freshly collected sediment. **C)** Fresh batch experiment
 244 – slurry experiment with freshly collected sediments (Bar-Or et al., 2017).

245

246
247

Table 1: Details of the three types of experiments: two-stage, semi-aerobic bioreactor and fresh batch experiments.

Experiment serial number (SN)	Experiment	Treatment	# of bottles	CH ₄ [ml]	¹³ CH ₄ [ml]	Fe ₂ O ₃ [mM]	Fe(OH) ₃ [mM]	MnO ₂ [mM]	NO ₂ ⁻ [mM]	NO ₃ ⁻ [mM]	AQDS [mM]	Humic substances [mM]	PCA [mM]	Fe-bearing nontronite (day) [gr]	Na ₂ -molybdate [mM]	BES [mM]	Acetylene [μL]	Temp [°C]	Duration [day]	Comments
1	Hematite	¹³ CH ₄ 13C-H ₂ -hematite	2 2	1 1	1 1	10												20 20	201	The methane that was added at the beginning of the experiment was not labelled, so ¹³ C-labeled methane was added after 105 days. Na ₂ -molybdate was added to one of the bottles on day 365
2	Magnetite	¹³ CH ₄ ¹³ CH ₄ +magnetite ¹³ CH ₄ +Fe(OH) ₃ Killed+ ¹³ CH ₄ +magnetite	2 2 2 1	1 1 1 1	1 1 1 1	10	10								1 1 1			16 16 16 16	447	Na ₂ -molybdate was added to one of the bottles on day 365
3	MnO ₂	¹³ CH ₄ ¹³ CH ₄ +MnO ₂ ¹³ CH ₄ +MnO ₂ (high conc.) ¹³ CH ₄ +hematite	2 2 2 2	1.2 1.2 0.5 1	1.2 1.2 0.5 1			10		1								20 20 20	201	200 μL ¹³ CH ₄ was added on day 1, then another 1 ml was added on day 24.
4	Nitrate	¹³ CH ₄ +NO ₂ ¹³ CH ₄ +NO ₂ (high conc.) ¹³ CH ₄ +NO ₂ (low conc.) Killed+ ¹³ CH ₄ +NO ₂ (high conc.) ¹³ CH ₄ ¹³ CH ₄ +NO ₂ (high conc.) ¹³ CH ₄ +NO ₂ (low conc.) Killed+ ¹³ CH ₄ +NO ₂ (high conc.) ¹³ CH ₄ +AQDS	1 3 2 2 3 2 2 2 3	0.5 0.5 0.5 1 0.5 0.5 1 1	0.5 0.5 0.5 1 0.5 0.5 1 1													20 20 20 20 20 20 20 20	306	
5	Nitrite	¹³ CH ₄ ¹³ CH ₄ +NO ₂ (high conc.) ¹³ CH ₄ +NO ₂ (low conc.) Killed+ ¹³ CH ₄ +NO ₂ (high conc.) ¹³ CH ₄ +AQDS	2 2 2 2	0.5 0.5 0.5 1	0.5 0.5 0.5 1	10			0.5 0.1 0.5		5 5							20 20 20 20	493	
6	AQDS	Killed+ ¹³ CH ₄ +AQDS	2	1	1													20	284	
7	Natural humic acids and clay	¹³ CH ₄ ¹³ CH ₄ +hematite ¹³ CH ₄ +humic acid ¹³ CH ₄ +clay Killed+ ¹³ CH ₄ +hematite	2 2 2 2 2	1 1 1 1 1	1 1 1 1 1													20 20 20 20	169	The head space of the experiment bottles was flushed with N ₂ on day 51 and ¹³ CH ₄ was added. This was done to match the the clay bottles.
8	Bromethanesulfonate (BES)	¹³ CH ₄ +hematite ¹³ CH ₄ +hematite+BES ¹³ CH ₄ +hematite	2 2 4	9 9 1	1 1 0.5	10							20				120	20	493	
9	Acetylene	¹³ CH ₄ +hematite+acetylene Killed+ ¹³ CH ₄ +hematite	2 2	0.5 1	0.5 1	10											120	20 20	321	Acetylene was injected to each bottle at different time points during the experiment.
10	No electron acceptor	No additions ¹³ CH ₄	3 3	1 1	1 1													20 20	147	
	Semi-bioreactor	¹³ CH ₄ ¹³ CH ₄ +hematite	15 15	15 15	15 15	10												16 16	345 677	
	Freshly collected sediment exp.	¹³ CH ₄ +hematite	0.05 0.05	0.05 0.05	0.05 0.05	20												20 20	467	

248

249 2.3 Analytical methods

250 2.3.1 Geochemical measurements

251 Measurements of $\delta^{13}\text{C}_{\text{DIC}}$ were performed on a DeltaV Advantage Thermo Scientific isotope-ratio mass-
252 spectrometer (IRMS). Results are reported referent to the Vienna Pee Dee Belemnite (VPDB) standard.
253 For these measurements, about 0.3 ml of filtered (0.22 μm) porewater was injected into a 12-ml glass
254 vial with a He atmosphere and 10 μl of H_3PO_4 85% to acidify all the DIC species to CO_2 (g). The
255 headspace autosampler (CTC Analytics; Type PC PAL) sampled the gas from the vials and measured
256 the $\delta^{13}\text{C}_{\text{DIC}}$ of the sample on the GasBench interface with a precision of ± 0.1 ‰. DIC was measured on
257 the IRMS using the peak height and a precision of 0.05 mM. Dissolved Fe(II) concentrations were
258 determined using the ferrozine method (Stookey, 1970) by a spectrophotometer at a 562-nm wavelength
259 with a detection limit of 1 $\mu\text{mol L}^{-1}$. A 100- μL headspace sample was taken for methane measurements
260 with a gas-tight syringe and was analyzed by gas chromatograph (Focus GC, Thermo) equipped with a
261 flame ionization detector (FID) and a packed column (Shincarbon ST) with a helium carrier gas (UHP)
262 and a detection limit of 1 nmol methane. Bottles to which acetylene was added were also measured by
263 GC for ethylene to determine the acetylene turnover with the N cycle.

264 2.3.2 Lipid analysis

265 A sub-set of samples (Table 3) was investigated for the assimilation of ^{13}C -labeled methane into polar
266 lipid-derived fatty acids (PLFAs) and intact ether lipid-derived hydrocarbons. A total lipid extract
267 (TLE) was obtained from 0.4 to 1.6 g of the freeze-dried sediment or incubated sediment slurry using a
268 modified Bligh and Dyer protocol (Sturt et al., 2004). Before extraction, 1 μg of 1,2-diheneicosanoyl-
269 *sn*-glycero-3-phosphocholine and 2-methyloctadecanoic acid were added as internal standards. PLFAs
270 in the TLE were converted to fatty acid methyl esters (FAMES) using saponification with KOH/MeOH
271 and derivatization with BF_3/MeOH (Elvert et al., 2003). Intact archaeal ether lipids in the TLE were
272 separated from the apolar archaeal lipid compounds using preparative liquid chromatography (Meador
273 et al., 2014) followed by ether cleavage with BBR_3 in dichloromethane forming hydrocarbons (Lin et
274 al., 2010). Both FAMES and ether-cleaved hydrocarbons were analyzed by GC-mass spectrometry (GC-
275 MS; Thermo Finnigan Trace GC coupled to a Trace MS) for identification and by GC-IRMS (Thermo
276 Scientific Trace GC coupled via a GC Isolink interface to a Delta V Plus) to determine $\delta^{13}\text{C}$ values by
277 using the column and temperature program settings described by Aepfler et al. (2019). The $\delta^{13}\text{C}$ values
278 are reported with an analytical precision better than 1‰ as determined by long-term measurements of
279 an *n*-alkane standard with known isotopic composition of each compound. Reported fatty acid isotope
280 data are corrected for the introduction of the methyl group during derivatization by mass balance
281 calculation similar to equation 1 (see below) using the measured $\delta^{13}\text{C}$ value of each FAME and the
282 known isotopic composition of methanol as input parameters.

283 2.3.3 Metagenomic analysis

284 For the metagenomic analyses, total genomic DNA was extracted from the semi-aerobic bioreactor with
 285 hematite addition (duplicate samples), pre-incubation slurries ($^{13}\text{CH}_4$ -only control, $^{13}\text{CH}_4$ + hematite)
 286 and their respective initial slurries (t0) by using the DNeasy PowerLyzer PowerSoil Kit (QIAGEN).
 287 Genomic DNA was eluted using 50 μl of elution buffer and stored at -20°C . Metagenomics libraries
 288 were prepared at the sequencing core facility at the University of Illinois at Chicago using the Nextera
 289 XT DNA library preparation kit (Illumina, USA). Between 19 and 40 million 2×150 bp paired-end
 290 reads per library were sequenced using Illumina NextSeq500. Metagenomes were co-assembled from
 291 the concatenated reads of all of the metagenomic libraries with Spades V3.12 (Bankevich et al., 2012;
 292 Nurk et al., 2013) after decontamination, quality filtering (QV= 10) and adapter-trimming with the
 293 BBDuk tool from the BBMap suite (Bushnell B, <http://sourceforge.net/projects/bbmap/>). Downstream
 294 analyses, including reading coverage estimates, automatic binning with maxbin (Wu et al., 2014) and
 295 metabat2 (Kang et al., 2019) bin refining with the DAS tool (Sieber et al., 2018), were performed within
 296 the SqueezeMeta framework (Tamames and Puente-Sánchez, 2019). GTDB-Tk was used to classify the
 297 metagenome-assembled genomes (MAGs) based on Genome Taxonomy Database release 95 (Parks et
 298 al., 2021). The principal component analysis biplot was constructed with Past V4.03 (Hammer et al.,
 299 2001).

300 2.3.4 Rate calculations

301 Methanogenesis rates were calculated from temporal changes in methane concentration in a
 302 representative pre-incubated slurry experiment (Fig. 2). The amount of methane oxidized was calculated
 303 by a simple mass balance calculation according to equations 1 and 2:

$$304 \quad x \times F^{13}\text{CH}_4 + (1 - x) \times FDI^{13}\text{C}_i = FDI^{13}\text{C}_f \quad (1)$$

$$305 \quad [\text{CH}_4]_{\text{ox}} = x \times [\text{DIC}]_f \quad (2)$$

306 The final DIC pool comprises two end members, the initial DIC pool and the oxidized ^{13}C - CH_4 . The
 307 term x denotes the fraction of oxidized ^{13}C - CH_4 , while $1-x$ denotes the fraction of the initial DIC pool
 308 out of the final DIC pool. $F^{13}\text{CH}_4$ is the fraction of ^{13}C out of the total CH_4 at t0 (i-initial), $FDI^{13}\text{C}_i$
 309 is the fraction of ^{13}C out of the total DIC at t0, and $FDI^{13}\text{C}_f$ is the fraction of ^{13}C out of the total DIC at
 310 t-final. $[\text{CH}_4]_{\text{ox}}$ is the amount (concentration in pore water) of the methane oxidized throughout the full
 311 incubation period, and $[\text{DIC}]_f$ is the DIC concentration at t-final. It was assumed that the isotopic
 312 composition of the labeled CH_4 did not change significantly throughout the incubation period.

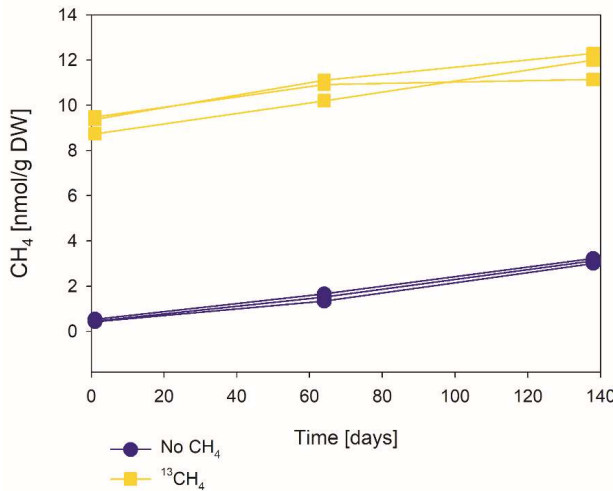
313 **3. Results**

314 In ten sets of slurry incubation experiments, we followed the progress of the methane oxidation process
 315 in Lake Kinneret methanogenic sediments in type A two-stage long-term incubations. This is by
 316 monitoring the changes in $\delta^{13}\text{C}_{\text{DIC}}$ values and by running metagenomic and specific isotope lipid

317 analyses. We also followed methane oxidation in a semi-continuous bioreactor system (type B) with
318 freshly collected sediments with or without the addition of hematite (Fig. 3). The results were compared
319 to those of fresh batch slurry incubations (type C) from the same methanogenic zone, presented by Bar-
320 Or et al. (2017) and Elul et al. (2021).

321 3.1 Geochemical trends in the long-term two-stage experiments

322 In the second stage (1:3 ratio of sediment to porewater) long-term batch slurry experiments (type A)
323 from the methanogenic zone, methanogenesis occurred with net methanogenesis rates of ~ 25 nmol g
324 dry weight (DW)⁻¹ d⁻¹ (Fig. 2, Table S2), which are similar to those of fresh incubation experiments
325 (Bar-Or et al., 2017). At the same time there was a conversion of ¹³C-methane to ¹³C-DIC in all the non-
326 killed slurries amended with ¹³C-methane, indicating significant AOM (Figs. 3 and 4). The $\delta^{13}\text{C}_{\text{DIC}}$
327 values of the “methane-only” control slurries reached as high values as 743‰. The average AOM rate
328 in the methane-only controls was 2.0 ± 0.4 nmol g DW⁻¹ d⁻¹ (Table 2). AOM was observed in these
329 geochemical experiments also with the addition of electron acceptors, and the potential of several
330 electron acceptors to perform and stimulate the AOM process is detailed below.



331

332 Figure 2: The change of methane concentrations with time of a representative incubated second stage long-term
333 slurry experiment, showing apparent net methanogenesis with average rate of 25 nmol g DW⁻¹ d⁻¹.

334 3.1.1 Metals as electron acceptors

335 Iron and manganese oxides were added as potential electron acceptors to the second stage long-term
336 slurries. The addition of hematite to three different experiments increased the $\delta^{13}\text{C}_{\text{DIC}}$ values over time
337 to 694‰, similar to the behavior of the methane-only controls, and in a different pattern than the fresh
338 experiments (Fig. 3). The average AOM rate in those two-stage treatments was 1.0 ± 0.3 nmol g DW⁻¹
339 d⁻¹ (Table 3). Magnetite amendments resulted in a minor increase of $\delta^{13}\text{C}_{\text{DIC}}$ values compared to the

340 methane-only controls (200‰ and 265‰, respectively, Fig. 4A) with an AOM rate of 1.8 nmol g DW⁻¹ d⁻¹. Amorphous iron amendments resulted in only a 22‰ increase in $\delta^{13}\text{C}_{\text{DIC}}$ and a lower AOM rate
341 (0.1 nmol g DW⁻¹ d⁻¹, Fig. 4A and Table 2). The addition of iron-bearing clay nontronite did not cause
342 any increase in the $\delta^{13}\text{C}_{\text{DIC}}$ values (Fig. 4B), but the concentration of dissolved Fe(II) increased
343 compared to the natural methane-only control (Fig. 5). Based on $\delta^{13}\text{C}_{\text{DIC}}$ estimates, no AOM was
344 detected 200 days after the addition of MnO₂ whereas the $\delta^{13}\text{C}_{\text{DIC}}$ values of the methane-only controls
345 increased to over 500‰ (Fig. 4F).
346

347 3.1.2 Sulfate as an electron acceptor

348 The involvement of sulfate in the AOM in the incubations was tested, even in the absence of detectable
349 sulfate in the methanogenic sediments. This is as sulfate could theoretically still be a short living
350 intermediate for the AOM process in an active cryptic sulfur cycle (Holmkvist et al., 2011). It was
351 quantified directly by adding Na-molybdate to the methane-only controls and the amended with
352 magnetite in the second stage long-term incubations (Fig. 4A). This addition did not affect the
353 increasing trend of $\delta^{13}\text{C}_{\text{DIC}}$ with time, and therefore, the AOM rates remained unchanged, similar to the
354 observation in the fresh batch incubations (Bar-Or et al., 2017).

355 3.1.3 Nitrate and nitrite as electron acceptors

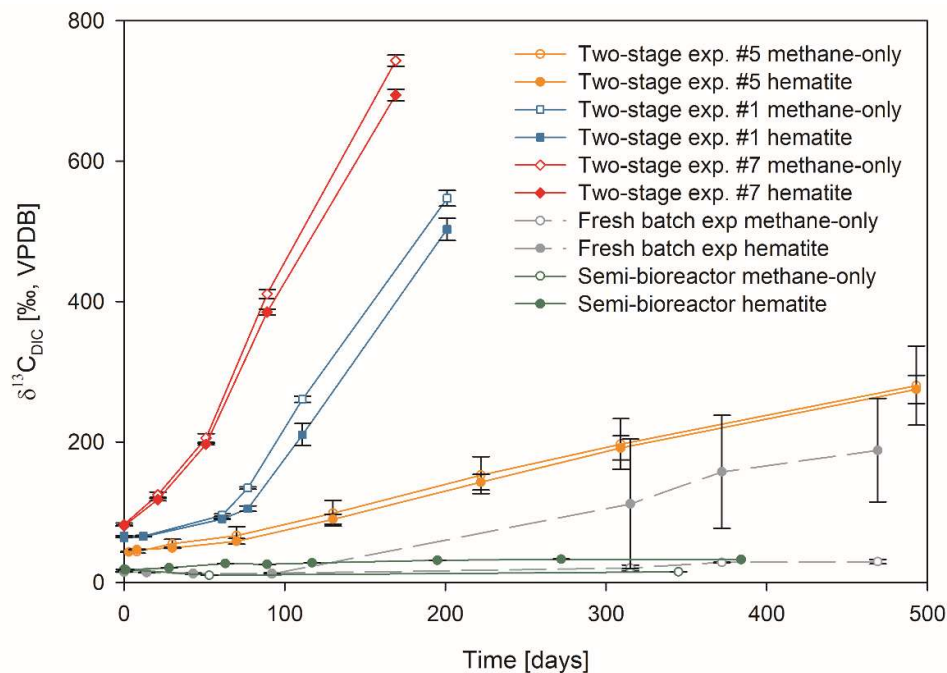
356 Nitrate and nitrite involvement in the AOM was tested for the feasibility of an active cryptic nitrogen
357 cycle, even in the absence of detectable amounts of nitrate and nitrite in the sediments (Nüsslein et al.,
358 2001; Sivan et al., 2011). Nitrate was added at two different concentrations (0.2 and 1 mM, Fig. 4C) to
359 the second stage long-term slurries amended with hematite, as these concentrations were shown
360 previously to promote AOM in other settings (Ettwig et al., 2010). The addition of hematite alone
361 increased the $\delta^{13}\text{C}_{\text{DIC}}$ values by ~200‰ during the 306 days of the experiment. The $\delta^{13}\text{C}_{\text{DIC}}$ in the bottles
362 with the addition of 1 mM nitrate, with and without hematite (Fig. 4C; the data points of the two
363 treatments are on top of each other), decreased from 43‰ at the beginning of the experiment to 35‰
364 after 306 days. The $\delta^{13}\text{C}_{\text{DIC}}$ in the bottles with the addition of 0.2 mM nitrate and hematite increased by
365 27‰ at the end of the experiment. Following the addition of 0.5 mM of nitrite, we observed no increase
366 in $\delta^{13}\text{C}_{\text{DIC}}$ values during the first 222 days (Fig. 4D), after which they increased from 34‰ to 54‰ by
367 the end of the experiment. The AOM rate of the high nitrite concentration treatment was 0.2 nmol g
368 DW⁻¹ d⁻¹ (Table 2). Following the addition of 0.1 mM nitrite, $\delta^{13}\text{C}_{\text{DIC}}$ increased only after 130 days to
369 158‰ on day 493. The AOM rate of the low nitrite concentration treatment was 0.5 nmol g DW⁻¹ d⁻¹.
370 In the methane-only controls, the $\delta^{13}\text{C}_{\text{DIC}}$ value reached a maximum of 330‰.

371 3.1.4 Organic compounds as electron acceptors

372 Two of the second stage long-term incubation experiments were amended with synthetic and natural
 373 organic electron acceptors to test the potential of organic electron acceptors. The addition of AQDS to
 374 slurries with and without hematite caused to a decrease in $\delta^{13}\text{C}_{\text{DIC}}$ values over the entire duration of the
 375 experiment (Fig. 4E). Dissolved Fe(II) increased by 50 μM in these treatments, while in those without
 376 AQDS, it exhibited an increase of 20 μM (Fig. S3). We further tested the effect of naturally occurring
 377 humic substances by using those isolated from a different natural lake. The results show that the $\delta^{13}\text{C}_{\text{DIC}}$
 378 values did not change at the beginning of the experiments (Fig. 4B), while a steep increase of $\sim 90 \mu\text{M}$
 379 in their Fe(II) concentration was observed (Fig. 5). After 20 days, the $\delta^{13}\text{C}_{\text{DIC}}$ values of these slurries
 380 started to increase dramatically from 84‰ to 150‰ with an AOM rate of 1.2 $\text{nmol g DW}^{-1} \text{d}^{-1}$ (Fig. 4B,
 381 Table 2). Dissolved Fe(II) concentrations mirrored the trend of $\delta^{13}\text{C}_{\text{DIC}}$ with a steep increase during the
 382 first 20 days followed by a decrease of 37 μM (Fig. 5).

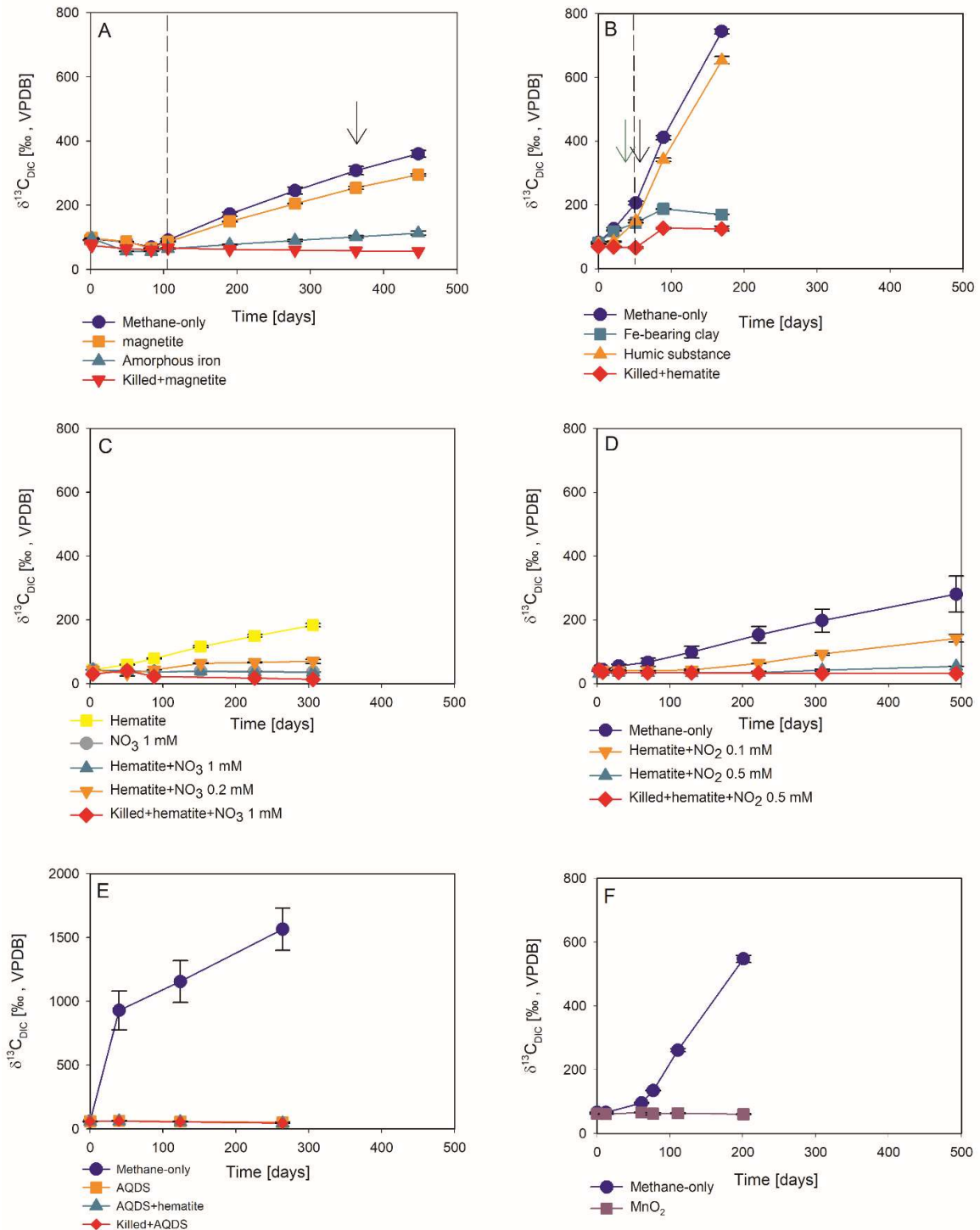
383 3.1.5 Metabolic pathways

384 To elucidate which metabolic processes drive AOM, we analyzed $\delta^{13}\text{C}_{\text{DIC}}$ following the addition of
 385 inhibitors to the second stage long-term slurries: i) BES, a specific inhibitor for methanogenesis (Nollet
 386 et al., 1997) and ii) acetylene, a non-specific inhibitor for methanogenesis and methanotrophy
 387 (Oremland and Capone, 1988). In both cases and similar to the killed control, labeled ^{13}C -DIC
 388 production was completely inhibited following the addition (Fig. 6). Though acetylene can also inhibit
 389 nitrogen cycling in some cases, it has been shown to result in the production of ethylene (Oremland and
 390 Capone, 1988). In our case, however, no ethylene was detected, supporting the conclusion that only the
 391 methanogenesis activity was inhibited.



392

393 Figure 3: Comparison of $\delta^{13}\text{C}_{\text{DIC}}$ values among the three types of experiments with ^{13}C -labeled methane addition:
 394 A) three two-stage slurry experiments (at the second stage of 1:3 ratio of sediment to porewater); B) the semi-
 395 continuous bioreactor experiment; and C) slurry batch experiment with freshly collected sediments (Bar-Or et al.,
 396 2017). In each experiment, two treatments are shown, with hematite (filled symbol) and without hematite (empty
 397 symbols). The error bars represent the average deviation of the mean of duplicate/triplicate bottles.



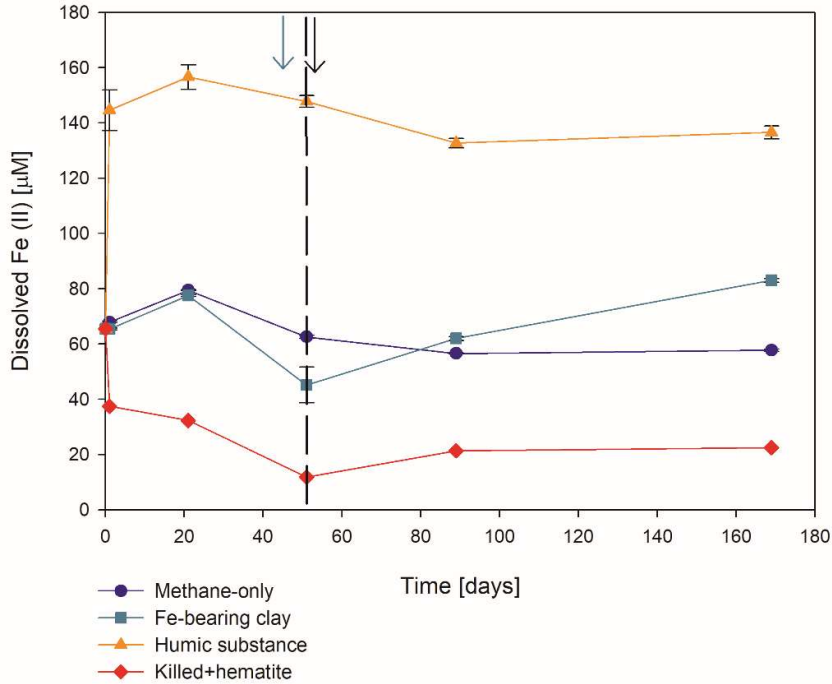
398

399 Figure 4: Potentials of different electron acceptors for AOM in Lake Kinneret in the two-stages long-term slurry
 400 experiments (at the second stage of 1:3 ratio of sediment to porewater) with of ¹³C -labeled methane and the
 401 following treatments: (A) with and without the addition of magnetite and amorphous iron (Fe(OH)₃). The dashed
 402 line represents the specific time of ¹³C -labeled methane addition. The black arrow represents the addition of Na-
 403 molybdate as an inhibitor for sulfate reduction. (B) with clay and natural humic substance. The green arrow
 404 represents the time clay was added to the relevant bottles, the dashed line represents the time the headspace of
 405 each bottle was flushed again with N₂, and the black arrow represents the second injection of 1 mL of ¹³C-labeled
 406 methane. (C) with the addition of hematite and two different concentrations of nitrate. (D) with the addition of
 407 hematite and two different concentrations of nitrite. (E) with the addition of AQDS. (F) with and without the
 408 addition of ¹³C-labeled methane to all of the bottles (see Table 1 for specific experimental details). Error bars
 409 represent the average deviations of the data points from their means of duplicate/triplicate bottles.

410 Table 2: AOM rates and AOM role in experiment A second stage slurries amended with ¹³C-labeled methane and
 411 different electron acceptors (assuming methanogenesis rate of 24.8 nmol g DW⁻¹ d⁻¹).

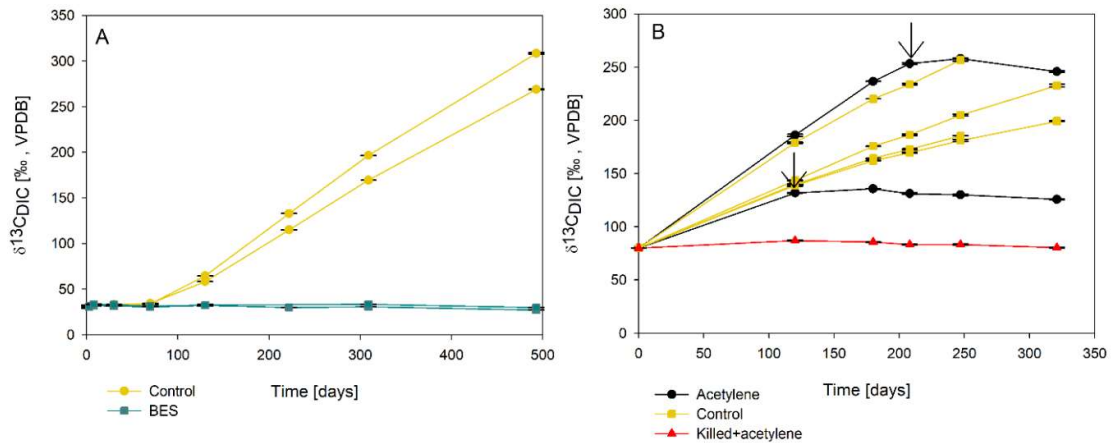
Experiment serial number (SN)	Treatment	AOM rate [nmol/g DW X d]	AOM/methanogenesis [%]
10	methane only	1.1	4.4
1	methane only	1.6	6.4
	methane+hematite	0.5	2.1
2	methane only	2.4	8.2
	methane+magnetite	1.8	6.3
	methane+amorphous iron	0.1	0.5
7	methane only	1.4	6.4
	methane+hematite	1.3	6.0
	methane+humics	1.2	5.4
5	methane only	1.0	4.6
	methane+hematite	1.0	4.6
	methane+hematite+nitrite 0.5 mM	0.2	0.8
	methane+hematite+nitrite 0.1 mM	0.5	2.1

412



413

414 Figure 5: Change in dissolved Fe(II) in the second stage of experiment No. 7 containing clay and natural humic
 415 acid. The green arrow represents the time at which clay was added to the specific bottles and those bottles were
 416 flushed with N₂, the dashed line represents the time at which the rest of the bottles were flushed, and the black
 417 arrow represents the time at which ¹³C-labeled methane was added again. Error bars represent the average of the
 418 absolute deviations of the data points from their means.

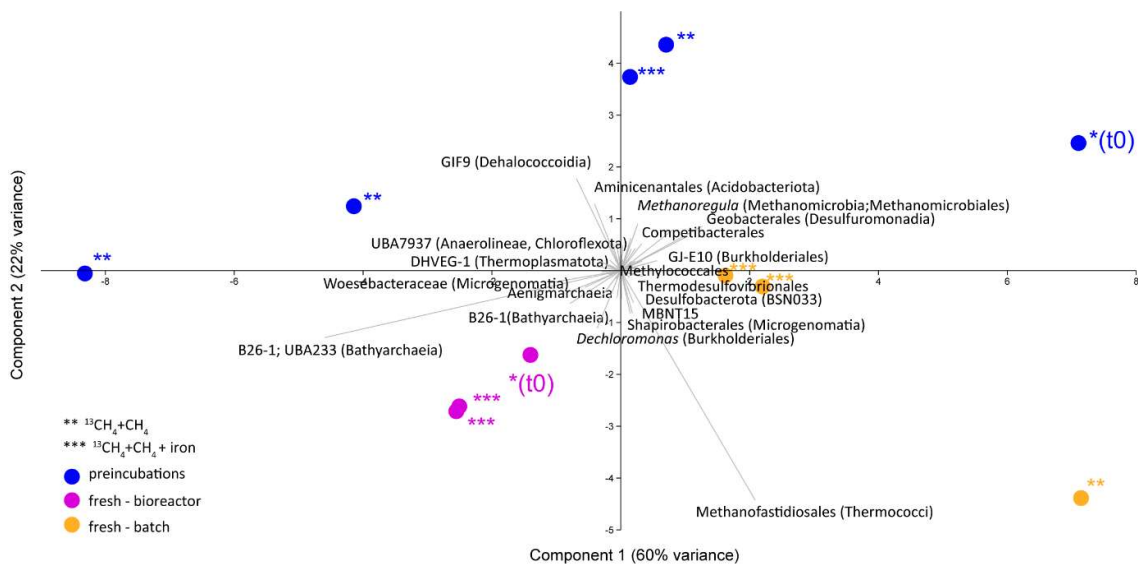


419

420 Figure 6: Change in $\delta^{13}\text{C}_{\text{DIC}}$ values over time in the second stage long-term sediment slurry incubations amended
 421 with hematite and ¹³C-labeled methane. (A) with/without BES and (B) with/without acetylene. Black arrows
 422 represent the time at which acetylene was injected into the experiment bottle. The error bars are smaller than the
 423 symbols.

424 **3.2 Microbial dynamics**

425 Analyses of taxonomy and coverage of metagenome-assembled genomes suggest that in the pre-
 426 incubated two-stage slurries, Bathyarchaea are the dominant archaea, together with putative
 427 methanogens such as Methanofastidiales (Thermococci), Methanoregulaceae (Methanomicrobia) and
 428 Methanotrichales (Methanosarcina) (Supplementary coverage table). Bona-fide ANME (ANME-1)
 429 were detected with substantial coverage of approximately 1 (the 27th most abundant from among the
 430 195 MAGs detected) in all of the treatments. Among the bacteria, the sulfate reducers Desulfobacterota
 431 and Thermodesulfovibrionales (Nitrospirota) were prominent together with the GIF9 Dehalococcoida
 432 lineage, which is known to metabolize chlorinated compounds in lake sediments (Biderre-Petit et al.,
 433 2016). Some Methyloirabilales (NC10) were found (average coverage of 0.32 ± 0.06), and no
 434 Methanoperedens were detected. Methylococcales methanotrophs were found in the natural sediments
 435 and the fresh batch and bioreactor incubations (average of 0.34 ± 0.02), in contrast to their average
 436 coverage of 0.09 ± 0.04 in the long-term incubations. Methylococcales comprised the *Methyloirabilis*,
 437 *Methyloirabilis* and *Methylobacter* genera (Supplementary coverage table). The methylotrophic partners
 438 of aerobic methanotrophs, *Methyloirabilis*, were found in fresh batch and bioreactor incubations, where
 439 *Methyloirabilis* was found, findings that are in line with those of previous studies that showed their
 440 association (Beck et al., 2013). Principal component analysis shows the grouping of long-term, pre-
 441 incubated slurries, semi-aerobic bioreactor incubations, and fresh batch experiments (Fig. 7),
 442 emphasizing the microbial dynamics over time.



443
 444 Figure 7: Principal component analysis comparison of three types of samples: long-term pre-incubated slurries
 445 (blue – experiment A), semi-continuous bioreactor (pink – experiment B) and fresh batch experiments (orange –
 446 experiment C). One asterisk represents t0, two asterisks denote methane-only treatments, three asterisks represent
 447 hematite treatment.

448 3.3 Lipid analysis

449 The $\delta^{13}\text{C}$ values of the archaeol-derived isoprenoid phytane were between -5 and -17‰ in the long-
450 term pre-incubated samples and thus showed ^{13}C -enrichment of 15 to 27‰ relative to the original
451 sediment. This is indicative of methane-derived carbon assimilation by archaea (Table 3). Acyclic
452 biphytane, derived mainly from caldarchaeol, exhibited a less pronounced ^{13}C -enrichment of 5-10‰.
453 For bacterial-derived fatty acids, $\delta^{13}\text{C}$ -values similarly shifted by up to 10‰ relative to the original
454 sediment. Nonetheless, one would have expected values to be extremely higher if aerobic
455 methanotrophs were active, as was previously indicated by strong ^{13}C -enrichments of up to 1,650‰ in
456 $\text{C}_{16:1\omega5c}$ observed in freshly incubated batch samples (Bar-Or et al., 2017).

457 Table 3: The $\delta^{13}\text{C}$ values (in ‰) of fatty acids and isoprenoid hydrocarbons from different experiments compared
458 to values obtained from the original sediment in the methanogenic zone.

Description	Temperature (°C)	Sampling (days)	Fatty acids		Hydrocarbons	
			$\text{C}_{16:1\omega9/8/7}$	$\text{C}_{16:1\omega5}$	Phytane	Biphytane
Pre-incubated slurry + $^{13}\text{CH}_4$ +hematite	20	411	-40	-43	-17	-23
Pre-incubated slurry + $^{13}\text{CH}_4$ (bottle A)	20	411	-40	-43	-13	-24
Pre-incubated slurry + $^{13}\text{CH}_4$ (bottle B)	20	1227	-36	-41	-5	-38
^a Fresh batch experiment+ $^{13}\text{CH}_4$ +hematite	20	470	610	1600	-14	-28
Semi-bioreactor+ $^{13}\text{CH}_4$ +hematite	16	382	n.d.	n.d.	n.d.	n.d.
Original sediment (28-30 cm)	14		-44	-51	-32	-33

^a Bar-Or et al., 2017
n.d. – Not detected

459

460 4. Discussion

461 4.1 Anaerobic oxidation of methane in the methanogenic sediment incubation experiments

462 The *in-situ* geochemical and microbial diversity profiles (Bar-Or et al., 2015) and the geochemical
463 (Sivan et al., 2011; Bar-Or et al., 2017; Fig. 3) and metagenomic (Elul et al., 2021) analyses of batch
464 incubations with fresh sediments provided strong support for the occurrence of Fe-AOM in sediments
465 of the methanogenic zone below 20 cm. Such profiles and alongside incubations showed an unexpected
466 presence of aerobic bacterial methanotrophs together with anaerobic microorganisms, such as
467 methanogens and iron reducers (Adler et al., 2011; Sivan et al., 2011; Bar-Or et al., 2015; Bar-Or et al.,
468 2017; Elul et al., 2021). These findings suggested that both *mcr* gene-bearing archaea and aerobic
469 bacterial methanotrophs mediate methane oxidation. In the current study, we have supportive evidence
470 of considerable AOM in the long-term incubations, even after the two treatment stages and considering
471 the low abundance of the microbial populations.

472 The data from the second stage incubations show a similar increasing trend in the $\delta^{13}\text{C}_{\text{DIC}}$ values of both
473 natural (methane-only) and the hematite amended treatments (Fig. 3). This deviates from our
474 observations during experiments B and C with fresh sediment, wherein higher $\delta^{13}\text{C}_{\text{DIC}}$ values were

475 obtained after the addition of hematite than in the methane-only treatment (Fig. 3 and Bar-Or et al.
476 (2017)). This was particularly dramatic in the batch slurries (experiment C), but it was also observed in
477 the semi-continuous bioreactor (experiment B). We assume that the observed difference in the
478 bioreactors would have been more pronounced if methane concentrations had been higher, but it is still
479 a significant finding. We also note that the difference between the bioreactors results may also be due
480 to the fact that each bioreactor community developed separately. The results of the type A experiments
481 (compared to those of types B and C) suggest that either hematite lacks the potential to stimulate the
482 AOM activity during the two-stage experiments or that there is enough natural Fe(III) in the sediments
483 to sustain the maximum potential of Fe-AOM. Below we characterize the AOM process in the long-
484 term, two-stage incubation experiments.

485 **4.2 Potential electron acceptors for AOM in the long-term two-stage incubation experiments**

486 Measurements of $\delta^{13}\text{C}_{\text{DIC}}$ show that the additions of magnetite, amorphous iron, clays and manganese
487 oxide in the second stage incubations resulted in a less pronounced increase in the $\delta^{13}\text{C}_{\text{DIC}}$ values
488 compared to those of the methane-only controls (Fig. 4). A possible explanation for the latter may be
489 that these metal oxides inhibit AOM, either directly or via a preference for organoclastic iron reduction
490 over Fe-AOM, which adds a natural, more negative carbon isotope signal from the organic materials
491 rather than the heavy carbon from the ^{13}C -labeled methane. Using mass-balance estimations in the
492 methane-only and in the amorphous iron treatments and considering the DIC concentrations and $\delta^{13}\text{C}_{\text{DIC}}$
493 values of the methane-only treatments at the beginning of the experiment (6 mM and 60‰, respectively)
494 and the values at the end (6.5 mM and 360‰, respectively), about 0.5 mM of the DIC was
495 added by the AOM of methane with $\delta^{13}\text{C}$ of ~4000‰. The DIC and $\delta^{13}\text{C}_{\text{DIC}}$ values of the amorphous
496 iron treatment at the beginning of the experiment were 5.4 mM and 60‰, respectively, and by the end
497 were 6.1 mM and 120‰, respectively. Assuming the same $\delta^{13}\text{C}$ of the added methane of 4000‰ and a
498 $\delta^{13}\text{C}_{\text{TOC}}$ of -30‰ (Sivan et al., 2011), 0.1 mM of the DIC should derive from AOM and 0.6 mM from
499 organoclastic metabolism. This means that adding amorphous iron to the system encouraged iron
500 reduction that was coupled to the oxidation of organic compounds other than methane. Intrinsic
501 microbes, particularly the commonly detected ex-deltaproteobacterial lineages such as Geobacterales,
502 may catalyze Fe(III) metal reduction, regardless of AOM (Xu et al., 2021). Manganese oxides are found
503 in very low abundance in Lake Kinneret sediments (0.1 %, Table S1 and Sivan et al., 2011). Thus, their
504 role in metal-AOM is likely minimal.

505 Sulfate concentrations in the methanogenic Lake Kinneret sediments have been below the detection
506 limit in years past, similar to their representation in the natural sediments we used for the incubations
507 (< 5 μM , Bar-Or et al., 2015; Elul et al., 2021). Sulfide concentrations have also been reported to be
508 minor (< 0.3 μM , Sivan et al., 2011). However, sulfate could theoretically still be a short-lived
509 intermediate for the AOM process, as pyrite and FeS precipitate in the top sediments, and cryptic

510 cycling via pyrite or FeS may replenish the sulfate, thus rendering it available for AOM (Bottrell et al.,
511 2000). The addition of Na-molybdate to the second stage slurries, including those amended with and
512 without magnetite, did not change the $\delta^{13}\text{C}_{\text{DIC}}$ dynamics, which remained similar to those from before
513 the addition of the inhibitor (Fig. 4A). This finding is in line with that in fresh batch sediment slurries
514 (Bar-Or et al., 2017) and suggests that sulfate is not a potent electron acceptor for AOM in this
515 environment. Furthermore, although sulfate-reducing bacteria were abundant, none of the reducers
516 belonged to the known clades of ANME-2d partners, which were connected previously to the Fe-S-CH₄
517 coupled AOM (Su et al., 2020; Mostovaya et al., 2021).

518 Nitrate and nitrite concentrations are also undetectable in the porewater of Lake Kinneret sediments
519 (Nüsslein et al., 2001; Sivan et al., 2011), but again may appear as short-lived intermediate products of
520 ammonium oxidation that is coupled to iron reduction (Tan et al., 2021; Ding et al., 2014; Shrestha et
521 al., 2009; Clement et al., 2005). We thus assessed the roles of nitrate and nitrite as electron acceptors in
522 the two-stage slurries. Our results indicate that the addition of nitrate did not promote AOM, likely due
523 to the absence of ANME-2d, which is known to use nitrate (Arshad et al., 2015; Haroon et al., 2013).
524 In the case of nitrite, even low concentrations appeared to delay the increase in $\delta^{13}\text{C}_{\text{DIC}}$ values,
525 suggesting that organoclastic denitrification outcompetes AOM, and despite the occurrence of
526 *Methylomirabilia*, the role of nitrite-AOM is not prominent in the two-stage incubations (Figs. 4C, D).

527 Humic substances may promote AOM by continuously shuttling electrons to metal oxides (Valenzuela
528 et al., 2019). Though humic substances were not measured directly in Lake Kinneret sediments, the
529 DOC concentrations in the methanogenic depth porewater were previously found to be high (~1.5 mM,
530 Adler et al., 2011), suggesting that they may play a role in AOM. Compared to the methane-only
531 treatments, the treatment with the synthetic humic analog AQDS caused an increase in dissolved Fe(II)
532 concentrations, but it did not cause ¹³C-DIC enrichment. This may be explained by the behavior of
533 AQDS as a strong electron shuttle in organoclastic iron reduction (Lovely et al., 1996), which produces
534 isotopically more negative carbon that masks the AOM signal (Fig. 4E, Fig. S3). Yet, as was done by
535 Valenzuela et al. (2017), the addition of natural humic substances did promote AOM, compared to the
536 rest of the electron acceptors tested, and may thus support AOM (Fig. 4B). In our incubations, the
537 natural humic substances promoted first the oxidation of organic matter by iron reduction, probably by
538 shuttling electrons from the broad spectrum of organic compounds to natural iron oxides (Figs. 4B and
539 5). When the availability of the iron oxides or the organic matter decreased, humic substances likely
540 took over to facilitate the AOM (Fig. 4B).

541 Overall, the results of our long-term two-stage experiments indicate that sulfate, nitrate, nitrite and
542 manganese oxides do not support AOM in the methanogenic sediments of Lake Kinneret. The candidate
543 electron acceptors for AOM in the long-term experiments are natural humic substances and/or the

544 naturally abundant iron minerals. Future experiments can simulate iron limitation and the involvement
545 of iron oxides in the AOM by removing natural iron oxides from the sediments.

546 **4.3 Main microbial players in the long-term two-stage slurries**

547 Methane oxidation in the pre-incubated Lake Kinneret sediments is likely mediated by either ANMEs
548 or methanogens, as the addition of BES and acetylene immediately stopped the AOM (Fig. 6) similar
549 to the results of the killed bottles and the BES treatment in the fresh batch experiment (Bar-Or et al.,
550 2017). Apart from methane-metabolizing, acetylene can inhibit nitrogen cycling, which results in
551 ethylene production (Oremland and Capone, 1988). This was not the case in our incubations, as no
552 ethylene was produced. The increase in $\delta^{13}\text{C}$ values in phytane and biphytane (Table 3) also indicates
553 the presence of active archaeal methanogens or ANMEs (Wegener et al., 2008; Kellermann et al., 2012;
554 Kurth et al., 2019).

555 Using the isotopic compositions of specific lipids and metagenomics, we identified a considerable
556 abundance of aerobic methanotrophs and methylotrophs in the fresh sediments, but not in the long-term
557 slurries (Table 3, Fig. 7). In the natural sediments, micro levels (nano molar) of oxygen could be trapped
558 in clays and slowly released to the porewater (Wang et al., 2018). However, if such micro levels of
559 oxygen still existed during the time of the pre-incubation, they were probably already exhausted.
560 Indeed, the results of our specific lipids and metagenomics analyses suggest that the aerobic
561 methanotrophs lineages play only a minor role in the long-term slurries, probably due to complete
562 depletion of the oxygen. The metagenomic data (Fig. 7, Supplementary coverage table) also indicate
563 that Bathyarchaea, which may be involved in methane metabolism (Evens et al., 2015), were enriched
564 in the bioreactor incubations, yet their role in Lake Kinneret AOM remains to be evaluated. We also
565 observed changes in the abundance of bacterial degraders of organic matter and necromass: for example,
566 GIF9 Dehalococcoidia, which can metabolize complex organic materials under methanogenic
567 conditions (Cheng et al., 2019; Hug et al., 2013), were most abundant in the long-term incubations (Fig.
568 7, Supplementary coverage table). Though ANME-1 are likely mediators of AOM in these sediments,
569 methane oxidation via reverse methanogenesis is feasible for some methanogens in Lake Kinneret
570 sediments (Elul et al., 2021).

571 **4.4 Mechanism of methane oxidation in the long-term two-stage incubations**

572 Our results indicate net methanogenesis in the two-stage incubation experiments with an average rate
573 of $25 \text{ nmol gr}^{-1} \text{ dry sediment day}^{-1}$ (Fig. 1 and Table S2), which are similar to those from fresh incubation
574 experiments (Bar-Or et al., 2017). This is despite the overall trend of increasing $\delta^{13}\text{C}_{\text{DIC}}$ values, a result
575 representing potential methane turnover (Figs. 3 and 4). A likely explanation for the presence of both
576 signals is an interplay between methane production and oxidation, which is possibly triggered by
577 reversal of the methanogenesis pathway in bonafide ANMEs or certain methanogens (Hallam et al.,

578 2004; Timmers et al., 2017). Due to the overall production of methane and the lack of intense
579 stimulation of AOM by any electron acceptor added, the increase in $\delta^{13}\text{C}_{\text{DIC}}$ values could theoretically
580 result from the occurrence of carbon back flux during methanogenesis, which is feasible in
581 environments that are close to thermodynamic equilibrium (Gropp et al., 2021). To test this, we used
582 DIC mass balance calculations to determine the strength of back flux in our incubations. Based on
583 equations 1 and 2, the observed level of ^{13}C -enrichment indicates that 3-8% of the ^{13}C -methane should
584 be converted into DIC. These estimates are orders of magnitude higher than the previously reported
585 values of 0.001-0.3% for methanogenesis back flux in cultures (Zehnder and Brock, 1979; Moran et al.,
586 2005), but they are in the same range as the back flux of 3.2 to 5.5% observed in ANME-enrichment
587 cultures (Holler et al., 2011). For the latter, however, modeling approaches from AOM-dominated
588 marine sediment samples and associated ANME enrichment cultures indicated the absence of net
589 methanogenesis (Yoshinaga et al., 2014; Chuang et al., 2019; Meister et al., 2019; Wegener et al., 2021).
590 Thus, it seems unlikely that back flux alone can account for the methane-to-DIC conversion in Lake
591 Kinneret sediments. Moreover, the occurrence of back flux alone in marine methanogenic sediments
592 with similar net methanogenesis rates and abundant methane-metabolizing archaea did not yield
593 considerable ^{13}C -enrichment in the DIC pool following sediment incubations (Sela-Adler et al., 2015;
594 Amiel, 2018; Vigderovich et al., 2019; Yorshansky, 2019) (Table S3). It is, therefore, less likely that
595 the observed DIC values in our study were sustained by methanogenesis back flux alone (without an
596 external electron acceptor) than by active AOM, which, in this case, is probably performed by ANME-
597 1 or by methanogens that perform reverse methanogenesis to some extent.

598 **Conclusions**

599 The previous results of the geochemical and microbial profiles and the fresh sediment incubations from
600 Lake Kinneret sediment constitute evidence of the occurrence of Fe-AOM, which removes about 10-
601 15% of the methane produced in the lake's sediment (Adler et al., 2011; Sivan et al., 2011). Anaerobic
602 archaea appear to be responsible for the methane turnover in these reduced sediments by reverse
603 methanogenesis, but aerobic Methylococcales may oxidize methane in these sediments as well. The co-
604 occurrence of aerobes and anaerobes in the natural environment may be the result of the presence of
605 undetected trace amounts of oxygen that are trapped at those depths in "nano-niches" or even in mineral
606 layers (Wang et al., 2018). This oxygen portion may not be removed by purging at the beginning of our
607 experiments but is rather slowly used by the methanotrophs for their survival. However, after two
608 incubation stages and intensive purging for a prolonged duration, only archaea remained active and
609 were involved in the observed methane turnover, consuming 3-8% of the methane produced. Thus, we
610 propose two modes of methanotrophy in Lake Kinneret sediments: i) methane oxidation performed by
611 Methylococcales species. This mode was observed only in the incubations with freshly collected
612 sediments (batch or bioreactor). ii) methane oxidation through reverse methanogenesis performed most

613 likely by ANME-1 or specific methanogens. This mode was observed in all incubation types and could
614 be a result of carbon back flux, however, the very high $\delta^{13}\text{C}_{\text{DIC}}$ signal points to a metabolic reaction.
615 This AOM is most probably coupled to the reduction of iron and/or humic substances, as terminal
616 electron acceptors or as electron shuttles stimulating the Fe-AOM.

617 **Competing interests.** The authors declare that they have no conflict of interest.

618 **Acknowledgments**

619 We would like to thank B. Sulimani and O. Tzabari from the Yigal Allon Kinneret Limnological
620 Laboratory for their onboard technical assistance. We thank all of O. Sivan's lab members for their help
621 during sampling and especially heartfelt thanks to N. Lotem for the invaluable assistance with the mass
622 balance calculations and the fruitful discussions and to E. Eliani-Russak for her technical assistance.
623 Many thanks to K. Hachmann from M. Elvert's lab for his help during lipid analysis and to J. Gropp for
624 insightful discussions about the back flux. This work was supported by ERC consolidator (818450) and
625 Israel Science Foundation (857-2016) grants awarded to O. Sivan. Funding for M. Elvert was provided
626 by the Deutsche Forschungsgemeinschaft (DFG) under Germany's Excellence Initiative/Strategy
627 through the Clusters of Excellence EXC 309 'The Ocean in the Earth System' (project no. 49926684)
628 and EXC 2077 'The Ocean Floor—Earth's Uncharted Interface' (project no. 390741601). Funding for
629 M. Rubin-Blum was provided by the Israel Science Foundation (913/19), the U.S.-Israel Binational
630 Science Foundation (2019055) and the Israel Ministry of Science and Technology (1126). H.
631 Vigderovich was supported by a student fellowship from the Israel Water Authority.

632

633 **References**

- 634 Adler, Michal, Eckert, W., & Sivan, O. (2011). Quantifying rates of methanogenesis and methanotrophy in Lake
635 Kinneret sediments (Israel) using porewater profiles. *Limnology and Oceanography*, *56*(4), 1525–1535.
636 <https://doi.org/10.4319/lo.2011.56.4.1525>
- 637 Aepfler, R. F., Bühring, S. I., & Elvert, M. (2019). Substrate characteristic bacterial fatty acid production based
638 on amino acid assimilation and transformation in marine sediments. *FEMS Microbiology Ecology*, *95*(10),
639 1–15. <https://doi.org/10.1093/femsec/fiz131>
- 640 Amiel, N. (2018). *Authigenic magnetite in deep sediments*. MsC thesis, Ben Gurion University of the Negev.
- 641 Arshad, A., Speth, D. R., De Graaf, R. M., Op den Camp, H. J. M., Jetten, M. S. M., & Welte, C. U. (2015). A
642 metagenomics-based metabolic model of nitrate-dependent anaerobic oxidation of methane by
643 Methanoperedens-like archaea. *Frontiers in Microbiology*, *6*(DEC), 1–14.
644 <https://doi.org/10.3389/fmicb.2015.01423>
- 645 Bai, Y. N., Wang, X. N., Wu, J., Lu, Y. Z., Fu, L., Zhang, F., Lau, T. C., & Zeng, R. J. (2019). Humic substances
646 as electron acceptors for anaerobic oxidation of methane driven by ANME-2d. *Water Research*, *164*,

- 647 114935. <https://doi.org/10.1016/j.watres.2019.114935>
- 648 Bankevich, A., Nurk, S., Antipov, D., Gurevich, A. a., Dvorkin, M., Kulikov, A. S., Lesin, V. M., Nicolenko, S.
649 I., Pham, S., Pribelski, A. D., Sirotkin, A. V., Vyahhi, N., Tesler, G., Aleksyev, A. M., & Pevzner, P. a.
650 (2012). SPAdes: A New Genome Assembly Algorithm and Its Applications to Single-Cell Sequencing.
651 *Journal of Computational Biology*, *19*(5), 455–477. <https://doi.org/10.1089/cmb.2012.0021>
- 652 Bar-Or, I., Ben-Dov, E., Kushmaro, A., Eckert, W., & Sivan, O. (2015). *Methane-related changes in*
653 *prokaryotes along geochemical profiles in sediments of Lake Kinneret (Israel) Methane-related changes*
654 *in prokaryotes along geochemical profiles in sediments of Lake Kinneret (Israel)*. (August).
655 <https://doi.org/10.5194/bg-12-2847-2015>
- 656 Bar-Or, I., Elvert, M., Eckert, W., Kushmaro, A., Vigderovich, H., Zhu, Q., Ben-Dov, E., & Sivan, O. (2017).
657 Iron-Coupled Anaerobic Oxidation of Methane Performed by a Mixed Bacterial-Archaeal Community
658 Based on Poorly Reactive Minerals. *Environmental Science & Technology*, *51*, 12293–12301.
659 <https://doi.org/10.1021/acs.est.7b03126>
- 660 Bastviken D. (2009). Methane. In: Likens G.E., ed. *Encyclopedia of Inland waters*, Oxford: Elsevier, 783–805.
661 <http://doi.org/10.1016/B978-012370626-3.00117-4>.
662
- 663 Beck, D. A. C., Kalyuzhnaya, M. G., Malfatti, S., Tringe, S. G., del Rio, T. G., Ivanova, N., Lidstrom, M. E., &
664 Chistoserdova, L. (2013). A metagenomic insight into freshwater methane-utilizing communities and
665 evidence for cooperation between the Methylococcaceae and the Methylophilaceae. *PeerJ*, *2013*(1), 1–23.
666 <https://doi.org/10.7717/peerj.23>
- 667 Biderre-Petit, C., Dugat-Bony, E., Mege, M., Parisot, N., Adrian, L., Moné, A., Denonfoux, J., Peyretailade, E.,
668 Debros. D., Boucher, D., Peyret, P. (2016). Distribution of Dehalococcoidia in the anaerobic deep water
669 of a remote meromictic crater lake and detection of Dehalococcoidia-derived reductive dehalogenase
670 homologous genes. *PLoS ONE*, *11*(1), 1–19. <https://doi.org/10.1371/journal.pone.0145558>
- 671 Boetius, A., Ravensschlag, K., Schubert, C. J., Rickert, D., Widdel, F., Gieseke, A., Amann, R., Jørgensen, B.B.,
672 Witte, U., & Pfannkuche, O. (2000). A marine microbial consortium apparently mediating AOM. *Nature*,
673 *407*(October), 623–626.
- 674 Bottrell, S. H., Parkes, R. J., Cragg, B. A., & Raiswell, R. (2000): Isotopic evidence for anoxic pyrite oxidation
675 and stimulation of bacterial sulphate reduction in marine sediments, *J. Geol. Soc. London*, *157*, 711–714.
676 <https://doi.org/10.1144/jgs.157.4.711>.
- 677 Cabrol, L., Thalasso, F., Gandois, L., Sepulveda-Jauregui, A., Martinez-Cruz, K., Teisserenc, R., Tananaev, N.,
678 Tveit, A., Svenning, M. M., & Barret, M. (2020). Anaerobic oxidation of methane and associated
679 microbiome in anoxic water of Northwestern Siberian lakes. *Science of the Total Environment*, *736*,
680 139588. <https://doi.org/10.1016/j.scitotenv.2020.139588>
- 681 Cai, C., Leu, A. O., Xie, G-J., Guo, J., Feng, Y., Zhao, J-X., Tyson, G. W., Yuan, Z., & Hu, S. (2018). A

682 methanotrophic archaeon couples anaerobic oxidation of methane to Fe(II) reduction. *ISME J*, 12, 1929-
683 1939. <http://dx.doi.org/10.1038/s41396-018-0109-x>

684 Cheng, L., Shi, S. bao, Yang, L., Zhang, Y., Dolfing, J., Sun, Y. ge, Liu, L., Li, Q., Tu, B., Dai, L., Shi, Q., &
685 Zhang, H. (2019). Preferential degradation of long-chain alkyl substituted hydrocarbons in heavy oil under
686 methanogenic conditions. *Organic Geochemistry*, 138. <https://doi.org/10.1016/j.orggeochem.2019.103927>

687 Chuang, P. C., Yang, T. F., Wallmann, K., Matsumoto, R., Hu, C. Y., Chen, H. W., Lin, S., Sun, CH., Li, HC.,
688 Wang, Y., & Dale, A. W. (2019). Carbon isotope exchange during anaerobic oxidation of methane (AOM)
689 in sediments of the northeastern South China Sea. *Geochimica et Cosmochimica Acta*, 246, 138–155.
690 <https://doi.org/10.1016/j.gca.2018.11.003>

691 Clement, J-C., Shrestha, J., Ehrenfeld, J. G., & Jaffe, P. R. (2005). Ammonium oxidation coupled to
692 dissimilatory iron reduction under anaerobic conditions in wetland soils. *Soil biology and biochemistry*,
693 37(12), 2323-2328. <http://doi.org/10.1016/j.soilbio.2005.03.027>

694 Conrad, R. (2009). The global methane cycle: Recent advances in understanding the microbial processes
695 involved. *Environmental Microbiology Reports*, 1(5), 285–292. [https://doi.org/10.1111/j.1758-](https://doi.org/10.1111/j.1758-2229.2009.00038.x)
696 2229.2009.00038.x

697 Crowe, S. A., Katsev, S., Leslie, K., Sturm, A., Magen, C., Nomosatryo, S., Pack, M. A., Kessler, J. D.,
698 Reeburgh, W. S., Roberts, J. a., González, L., Douglas Haffner, G., Mucci, A., Sundby, B., & Fowle, D.
699 A. (2011). The methane cycle in ferruginous Lake Matano. *Geobiology*, 9(1), 61-78.
700 <http://doi.org/10.1111/j.1472-4669.2010.00257.x>

701 Damgaard, L. R., Revsbech, N. P., & Reichardt, W. (1998). Use of an oxygen-insensitive microscale biosensor
702 for methane to measure methane concentration profiles in a rice paddy. *Applied and Environmental*
703 *Microbiology*, 64(3), 864-870. <http://doi.org/10.1128/aem.64.3.864-870.1998>

704 Dershwitz, P., Bandow, N. L., Yang, J., Semrau, J. D., McEllistrem, M. T., Heinze, R. A., Fonseca, M.,
705 Ledesma, J. C., Jennett, J. R., DiSpirito, A. M., Athwal, N. S., Hargrove, M. S., Bobik, T. A., Zischka, H.,
706 & DiSpirito, A. A. (2021). Oxygen Generation via Water Splitting by a Novel Biogenic Metal Ion-
707 Binding Compound. *Applied and Environmental Microbiology*, 87(14), 1–14.
708 <https://doi.org/10.1128/aem.00286-21>

709 Ding, L. J., An, X. L., Li, S., Zhang, G. L., & Zhu, Y. G. (2014). Nitrogen loss through anaerobic ammonium
710 oxidation coupled to iron reduction from paddy soils in a chronosequence. *Environmental Science and*
711 *Technology*, 48(18), 10641-10647. <http://doi.org/10.1021/es503113s>

712 Elul, M., Rubin-Blum, M., Ronen, Z., Bar-Or, I., Eckert, W., & Sivan, O. (2021). Metagenomic insights into the
713 metabolism of microbial communities that mediate iron and methane cycling in Lake Kinneret sediments.
714 *Biogeosciences Discussions*, 1–24. <https://doi.org/10.5194/bg-2020-329>

715 Elvert, M., Boetius, A., Knittel, K., & Jørgensen, B. B. (2003). Characterization of specific membrane fatty
716 acids as chemotaxonomic markers for sulfate-reducing bacteria involved in anaerobic oxidation of
717 methane. *Geomicrobiology Journal*, 20(4), 403–419. <https://doi.org/10.1080/01490450303894>

718 Ettwig, K. F., Zhu, B., Speth, D., Keltjens, J. T., Jetten, M. S. M., & Kartal, B. (2016). Archaea catalyze iron-

719 dependent anaerobic oxidation of methane. *PNAS*, *113*(45), 12792-12796.
720 <http://doi.org/10.1073/pnas.1609534113>

721 Ettwig, Katharina F, Butler, M. K., Le Paslier, D., Pelletier, E., Mangenot, S., Kuypers, M. M. M., Schreiber, F.,
722 Dutilh, B. E., Zedelius, J., de Beer, D. Gloerich, J., Wessels, H. J. C. T., van Alen, T., Luesken, F., Wu,
723 M. L., van de Pas-Schoonen K. T., Op den Camp, H. J. M., Jansen-Megens, E. M., Francoijs, KJ.,
724 Stunnenberg, H., Weissenbach, J., Jetten, M. S. M., & Strous, M. (2010). Nitrite-driven anaerobic
725 methane oxidation by oxygenic bacteria. *Nature*, *464*(7288), 543–548.
726 <https://doi.org/10.1038/nature08883>

727 Evans, P. N., Parks, D. H., Chadwick, G. L., Robbins, S. J., Orphan V. J., Golding, S. D., & Tyson, G. W.
728 (2015). *Science*. *350*(6259), 434-438. <http://doi.org/10.1126/science.aac7745>.

729
730 Fan, L., Dippold, M. A., Ge, T., Wu, J., Thiel, V., Kuzyakov, Y., & Dorodnikov, M. (2020). Anaerobic
731 oxidation of methane in paddy soil: Role of electron acceptors and fertilization in mitigating CH₄ fluxes.
732 *Soil Biology and Biochemistry*, *141*, 107685. <https://doi.org/10.1016/j.soilbio.2019.107685>

733 Froelich, P. N., Klinkhammer, G. P., Lender, M. L., Luedtke, N. A., Heath, G. R., Cullen, D., Dauphin, P.,
734 Hammond, D., Hartman, B., & Maynard, V. (1979). *Geochemica et Cosmochimica Acta*, *43*, 1075-1090.
735 [https://doi.org/10.1016/0016-7037\(79\)90095-4](https://doi.org/10.1016/0016-7037(79)90095-4)

736 Gropp, J., Iron, M. A., & Halevy, I. (2021). Theoretical estimates of equilibrium carbon and hydrogen isotope
737 effects in microbial methane production and anaerobic oxidation of methane. *Geochimica et*
738 *Cosmochimica Acta*, *295*, 237–264. <https://doi.org/10.1016/j.gca.2020.10.018>

739 Hallam, S. J., Putnam, N., Preston, C. M., Detter, J. C., Rokhsar, D., Richardson, P. H., & DeLong, E. F. (2004).
740 Reverse methanogenesis: Testing the hypothesis with environmental genomics. *Science*, *305*(5689),
741 1457–1462. <https://doi.org/10.1126/science.1100025>

742 Hammer, Ø., Harper, D. A. T., & Ryan, P. D. (2001) Past: paleontological statistics software package for
743 education and data analysis. *Paleontologia-Electronica*. *4* (1), 9.
744

745 Haroon, M. F., Hu, S., Shi, Y., Imelfort, M., Keller, J., Hugenholtz, P., Yuan, Z., & Tyson, G. W. (2013).
746 Anaerobic oxidation of methane coupled to nitrate reduction in a novel archaeal lineage. *Nature*,
747 *500*(7464), 567–570. <https://doi.org/10.1038/nature12375>

748 Hoehler, T. M., Alperin, M. J., Albert, D. B., & Martens, C. S. (1994). Field and laboratory, evidence for a
749 methane-sulfate reducer consortium.pdf. *Global Biogeochemical Cycles*, *8*(4), 451–463.

750 Holler, T., Wegener, G., Niemann, H., Deusner, C., Ferdelman, T. G., Boetius, A., Brunner, B., & Widdel, F.
751 (2011). Carbon and sulfur back flux during anaerobic microbial oxidation of methane and coupled sulfate
752 reduction. *Proceedings of the National Academy of Sciences of the United States of America*, *108*(52).
753 <https://doi.org/10.1073/pnas.1106032108>

754 Holmkvist, L., Ferdelman, T. G., & Jørgensen, B. B. (2011). A cryptic sulfur cycle driven by iron in the
755 methane zone of marine sediment (Aarhus Bay, Denmark). *Geochimica et Cosmochimica Acta*, *75*(12),
756 3581–3599. <https://doi.org/10.1016/j.gca.2011.03.033>

- 757 Hug, L. A., Castelle, C. J., Wrighton, K. C., Thomas, B. C., Sharon, I., Frischkorn, K. R., Williams, K. H.,
758 Tringe, S. G., & Banfield, J. F. (2013). Community genomic analyses constrain the distribution of
759 metabolic traits across the Chloroflexi phylum and indicate roles in sediment carbon cycling. *Microbiome*,
760 *1*(1), 1–17. <https://doi.org/10.1186/2049-2618-1-22>
- 761 Kang, D. D., Li, F., Kirton, E., Thomas, A., Egan, R., An, H., & Wang, Z. (2019). MetaBAT 2: An adaptive
762 binning algorithm for robust and efficient genome reconstruction from metagenome assemblies. *PeerJ*,
763 *2019*(7), 1–13. <https://doi.org/10.7717/peerj.7359>
- 764 Kellermann, M. Y., Wegener, G., Elvert, M., Yoshinaga, M. Y., Lin, Y. S., Holler, T., Mollar, P. X., Knittel K.,
765 & Hinrichs, K. U. (2012). Autotrophy as a predominant mode of carbon fixation in anaerobic methane-
766 oxidizing microbial communities. *Proceedings of the National Academy of Sciences of the USA* *109*(47),
767 19321–19326. doi:10.1073/pnas.1208795109.
- 768 Kits, K. D., Klotz, M. G., & Stein, L. Y. (2015). Methane oxidation coupled to nitrate reduction under hypoxia
769 by the Gammaproteobacterium *Methylomonas denitrificans*, sp. nov. type strain FJG1. *Environmental*
770 *Microbiology*, *17*(9), 3219–3232. <https://doi.org/10.1111/1462-2920.12772>
- 771 Knittel, K., & Boetius, A. (2009). Anaerobic oxidation of methane: Progress with an unknown process. *Annual*
772 *Review of Microbiology*, *63*, 311–334. <https://doi.org/10.1146/annurev.micro.61.080706.093130>
- 773 Kurth, J.M., Nadine T Smit, Stefanie Berger, Stefan Schouten, Mike S M Jetten, Cornelia U Welte, Anaerobic
774 methanotrophic archaea of the ANME-2d clade feature lipid composition that differs from other ANME
775 archaea, *FEMS Microbiology Ecology*, Volume 95, Issue 7, July 2019, fiz082.
- 776 Li, X., Hou, L., Liu, M., Zheng, Y., Yin, G., Lin, X., Cheng, L., Li, Y., & Hu, X. (2015). Evidence of Nitrogen
777 Loss from Anaerobic Ammonium Oxidation Coupled with Ferric Iron Reduction in an Intertidal Wetland.
778 *Environmental Science and Technology*, *49*(19), 11560–11568. <https://doi.org/10.1021/acs.est.5b03419>
- 779 Lin, Y. S., Lipp, J. S., Yoshinaga, M. Y., Lin, S. H., Elvert, M., & Hinrichs, K. U. (2010). Intramolecular stable
780 carbon isotopic analysis of archaeal glycosyl tetraether lipids. *Rapid Communications in Mass*
781 *Spectrometry*, *24*(19), 2817–2826. <https://doi.org/10.1002/rcm.4707>Lovley, D. R., & Klug, M. J. (1983).
782 Sulfate reducers can outcompete methanogens at freshwater sulfate concentrations. *Applied and*
783 *Environmental Microbiology*, *45*(1), 187–192. <https://doi.org/10.1128/aem.45.1.187-192.1983>
- 784 Lovley, D. R., Coates, J. D., Blunt-Harris, E. L., Phillips, E. J. P., & Woodward, J. C. (1996). Humic substances
785 as electron acceptors for microbial respiration. *Nature*, *382*, 445–448. <https://doi.org/10.1038/382445a0>
- 786 Lu, Y. Z., Fu, L., Ding, J., Ding, Z. W., Li, N., & Zeng, R. J. (2016). Cr(VI) reduction coupled with anaerobic
787 oxidation of methane in a laboratory reactor. *Water Research*, *102*, 445–452.
788 <http://doi.org/10.1016/j.watres.2016.06.065>
- 789 Martinez-cruz, K., Leewis, M., Charold, I., Sepulveda-jauregui, A., Walter, K., Thalasso, F., & Beth, M. (2017).
790 Science of the Total Environment Anaerobic oxidation of methane by aerobic methanotrophs in sub-
791 Arctic lake sediments. *Science of the Total Environment*, *607–608*, 23–31.
792 <https://doi.org/10.1016/j.scitotenv.2017.06.187>

- 793 Meador, T. B., Gagen, E. J., Loscar, M. E., Goldhammer, T., Yoshinaga, M. Y., Wendt, J., Thomm, M., &
794 Hinrichs, K. U. (2014). *Thermococcus kodakarensis* modulates its polar membrane lipids and elemental
795 composition according to growth stage and phosphate availability. *Frontiers in Microbiology*, 5(JAN), 1–
796 13. <https://doi.org/10.3389/fmicb.2014.00010>
- 797 Meister, P., Liu, B., Khalili, A., Böttcher, M. E., & Jørgensen, B. B. (2019). Factors controlling the carbon
798 isotope composition of dissolved inorganic carbon and methane in marine porewater: An evaluation by
799 reaction-transport modelling. *Journal of Marine Systems*, 200(August), 103227.
800 <https://doi.org/10.1016/j.jmarsys.2019.103227>
- 801 Moran, J. J., House, C. H., Freeman, K. H., & Ferry, J. G. (2005). Trace methane oxidation studied in several
802 Euryarchaeota under diverse conditions. *Archaea*, 1(5), 303–309. <https://doi.org/10.1155/2005/650670>
- 803 Mosrovaya, A., Wind-Hansen, M., Rousteau, P., Bristow, L. A., & Thamdrup, B. (2021) Sulfate- and iron-
804 dependent anaerobic methane oxidation occurring side-by-side in freshwater lake sediments. *Limnology
805 and Oceanography*. <https://doi.org/10.1002/lno.11988>
- 806 Nollet, L., Demeyer, D., & Verstraete, W. (1997). Effect of 2-bromoethanesulfonic acid and *Peptostreptococcus*
807 *productus* ATCC 35244 addition on stimulation of reductive acetogenesis in the ruminal ecosystem by
808 selective inhibition of methanogenesis. *Applied and Environmental Microbiology*, 63(1), 194–200.
809 <https://doi.org/10.1128/aem.63.1.194-200.1997>
- 810 Norði, K. á., Thamdrup B., & Schubert, C. J. (2013). Anaerobic oxidation of methane in an iron-rich Danish
811 freshwater lake sediment. *Limnology and Oceanography*, 58(2), 546-554.
812 <http://doi.org/10.4319/lo.2013.58.2.0546>
- 813 Norði, K. á., & Thamdrup B. (2014). Nitrate-dependent anaerobic methane oxidation in freshwater sediment.
814 *Geochimica et Cosmochimica Acta*, 132, 141-150. <http://doi.org/10.1016/j.gca.2014.01.032>
- 815 Nurk, S., Bankevich, A., & Antipov, D. (2013). Assembling genomes and mini-metagenomes from highly
816 chimeric reads. *Research in Computational Molecular Biology*, 158–170. [https://doi.org/10.1007/978-3-
817 642-37195-0](https://doi.org/10.1007/978-3-642-37195-0)
- 818 Nüsslein, B., Chin, K. J., Eckert, W., & Conrad, R. (2001). Evidence for anaerobic syntrophic acetate oxidation
819 during methane production in the profundal sediment of subtropical Lake Kinneret (Israel). *Environmental
820 Microbiology*, 3(7), 460–470. <https://doi.org/10.1046/j.1462-2920.2001.00215.x>
- 821 Orembland, R. S., & Capone, D. G. (1988). *Use of "Specific" Inhibitors in Biogeochemistry and Microbial
822 Ecology* (Vol. 10). <https://doi.org/10.2307/4514>
- 823 Orphan, V. J., House, C. H., & Hinrichs, K. (2001). Methane-Consuming Archaea Revealed by Directly
824 Coupled Isotopic and Phylogenetic Analysis. *Science*, 293(July), 484–488.
825 <https://doi.org/10.1126/science.1061338>
- 826 Oswald, K., Milucka, J., Brand, A., Hach, P., Littmann, S., Wehrli, B., Albersten, M., Daims, H., Wagner, M.,
827 Kuypers, M. M. M., Schubert, C. J., & Milucka, J. (2016). Aerobic gamma-proteobacterial methanotrophs

- 828 mitigate methane emissions from oxic and anoxic lake waters. *Limnology and Oceanography*, 61, S101–
829 S118. <https://doi.org/10.1002/lno.10312>
- 830 Parks, D. H., Chuvochina, M., Rinke, C., Mussig, A. J., Chaumeil, P.-A., & Hugenholtz, P. (2021) GTDB: an
831 ongoing census of bacterial and archaeal diversity through a phylogenetically consistent, rank
832 normalized and complete genome-based taxonomy. *Nucleic Acids Research*, 202, 1-10.
833 <http://doi.org/10.1093/nar/gkab776>
- 834 Raghoebarsing, A. A., Pol, A., Van De Pas-Schoonen, K. T., Smolders, A. J. P., Ettwig, K. F., Rijnstra, W. I. C.,
835 Schouten, S., Sinninghe Damsté, J. S., Op den Camp, H. J. M., Jetten, M. S. M., & Strous, M. (2006). A
836 microbial consortium couples anaerobic methane oxidation to denitrification. *Nature*, 440(7086), 918–
837 921. <https://doi.org/10.1038/nature04617>
- 838 Reeburgh, W. S. (2007). Oceanic Methane Biogeochemistry. *ChemInform*, 38(20), 486–513.
839 <https://doi.org/10.1002/chin.200720267>
- 840 Rosentreter, J. A., Borges, A. V., Deemer, B. R., Holgerson, M. A., Liu, S., Song, C., Melack, J., Raymond, P.
841 A., Duarte, C. M., Allen, G. H., Olefeldt, D., Poulter, B., Battin, T. I., & Eyre, B. D. (2021). *Nature*
842 *geoscience*, 14(4), 225-230. <http://doi.org/10.1038/s41561-021-00715-2>
- 843 Saunio, M., Stavert, A. R., Poulter, B., Bousquet, P., Canadell, J. G., Jackson, R. B., Raymond, P. A.,
844 Dlugokencky, E. J., Houweling, S., Patra, P. K., Ciais, P., Arora, V. K., Bastviken, D., Bergamaschi, P.,
845 Blake, D. R., Brailsford, G., Bruhwiler, L., Carlson, K. M., Carrol, M., Castaldi, S., Chandra, N.,
846 Crevoisier, C., Crill, P. M., Covey, K., Curry, C. L., Etiope, G., Frankenberg, C., Gedney, N., Hegglin, M.
847 I., Höglund-Isaksson, L., Hugelius, G., Ishizawa, M., Ito, A., Janssens-Maenhout, G., Jensen, K. M., Joos,
848 F., Kleinen, T., Krummel, P. B., Langenfelds, R. L., Laruelle, G. G., Liu, L., Machida, T., Maksyutov, S.,
849 McDonald, K. C., McNorton, J., Miller, P. A., Melton, J. R., Morino, I., Müller, J., Murguia-Flores, F.,
850 Naik, V., Niwa, Y., Noce, S., O'Doherty, S., Parker, R. J., Peng, C., Peng, S., Peters, G. P., Prigent, C.,
851 Prinn, R., Ramonet, M., Regnier, P., Riley, W. J., Rosentreter, J. A., Segers, A., Simpson, I. J., Shi, H.,
852 Smith, S. J., Steele, L. P., Thornton, B. F., Tian, H., Tohjima, Y., Tubiello, F. N., Tsuruta, A., Viovy, N.,
853 Voulgarakis, A., Weber, T. S., van Weele, M., van der Werf, G. R., Weiss, R. F., Worthy, D., Wunch, D.,
854 Yin, Y., Yoshida, Y., Zhang, W., Zhang, Z., Zhao, Y., Zheng, B., Zhu, Q., Zhu, Q., and Zhuang, Q.: The
855 Global Methane Budget 2000–2017, *Earth Syst. Sci. Data*, 12, 1561–1623, <https://doi.org/10.5194/essd-12-1561-2020>, 2020.
- 857 Schubert, C. J., Vazquez, F., Lösekann-Behrens, T., Knittel, K., Tonolla, M., & Boetius, A. (2011). Evidence for
858 anaerobic oxidation of methane in sediments of a freshwater system (Lago di Cadagno). *FEMS*
859 *Microbiology Ecology*, 76(1), 26-38. <http://doi.org/10.1111/j.1574-6941.2010.01036.x>
- 860 Segarra, K. E. A., Schubotz, F., Samarkin, V., Yoshinaga, M. Y., Hinrichs, K-U., & Joye, S. B. (2015). *Nature*
861 *communications*, 6(may), 1-8. <http://dx.doi.org/10.1038/ncomms8477>
- 862 Sela-Adler, M., Herut, B., Bar-Or, I., Antler, G., Eliani-Russak, E., Levy, E., Makovsky, Y., & Sivan, O.
863 (2015). Geochemical evidence for biogenic methane production and consumption in the shallow
864 sediments of the SE Mediterranean shelf (Israel). *Continental Shelf Research*, 101, 117–124.
865 <https://doi.org/10.1016/j.csr.2015.04.001>

866 Shrestha, J., Rich, J. J., Ehrenfeld, J. G., & Jaffe, P. R. (2009). Oxidation of ammonium to nitrite under iron-
867 reducing conditions in wetland soils: Laboratory, field demonstrations, and push-pull rate determination.
868 *Soil Science*, 174(3), 156-164. <http://doi.org/10.1097/SS.0b013e3181988bf>

869 Shuai, W., & Jaffé, P. R. (2019). Anaerobic ammonium oxidation coupled to iron reduction in constructed
870 wetland mesocosms. *Science of the Total Environment*, 648, 984–992.
871 <https://doi.org/10.1016/j.scitotenv.2018.08.189>

872 Sieber, C. M. K., Probst, A. J., Sharrar, A., Thomas, B. C., Hess, M., Tringe, S. G., & Banfield, J. F. (2018).
873 Recovery of genomes from metagenomes via a dereplication, aggregation and scoring strategy. *Nature*
874 *Microbiology*, 3(7), 836–843. <https://doi.org/10.1038/s41564-018-0171-1>

875 Sinke, A. J. C., Cornelese, A. A., Cappenberg, T. E., & Zehnder, A. J. B. (1992). Seasonal variation in sulfate
876 reduction and methanogenesis in peaty sediments of eutrophic Lake Loosdrecht, The Netherlands.
877 *Biogeochemistry*, 16(1), 43-61. <http://doi.org/10.1007/BF02402262>

878 Sivan, O, Adler, M., Pearson, A., Gelman, F., Bar-Or, I., John, S. G., & Eckert, W. (2011). Geochemical
879 evidence for iron-mediated anaerobic oxidation of methane. *Limnology and Oceanography*, 56(4), 1536–
880 1544.

881 Stookey, L. L. (1970). Ferrozine-a new spectrophotometric reagent for iron. *Analytical Chemistry*, 42(7), 779–
882 781. <https://doi.org/10.1021/ac60289a016>

883 Sturt, H. F., Summons, R. E., Smith, K., Elvert, M., & Hinrichs, K. U. (2004). Intact polar membrane lipids in
884 prokaryotes and sediments deciphered by high-performance liquid chromatography/electrospray
885 ionization multistage mass spectrometry - New biomarkers for biogeochemistry and microbial ecology.
886 *Rapid Communications in Mass Spectrometry*, 18(6), 617–628. <https://doi.org/10.1002/rcm.1378>

887 Su, G., Zopfi, J., Yao, H., Steinle, L., Niemann, H., & Lehmann, M. F. (2020). Manganese/iron-supported
888 sulfate-dependent anaerobic oxidation of methane by archaea in lake sediments. *Limnology and*
889 *Oceanography*, 65(4), 863–875. <https://doi.org/10.1002/lno.11354>

890 Tamames, J., & Puente-Sánchez, F. (2019). SqueezeMeta, A Highly Portable, Fully Automatic Metagenomic
891 Analysis Pipeline. *Frontiers in Microbiology*, 9. <https://doi.org/10.3389/fmicb.2018.03349>

892 Tan, X., Xie, G. J., Nie, W. B., Xing, D-F., Liu, B. F., Ding, J., & Ren, N. Q. (2021). Fe(III)-mediated anaerobic
893 ammonium oxidation: A novel microbial nitrogen cycle pathway and potential applications. *Critical*
894 *Reviews in Environmental Science and Technology*. <https://doi.org/10.1080/10643389.2021.1903788>

895 Timmers, P. H. A., Welte, C. U., Koehorst, J. J., Plugge, C. M., Jetten, M. S. M., & Stams, A. J. M. (2017).
896 Reverse Methanogenesis and Respiration in Methanotrophic Archaea. *Archaea*, 2017(Figure 1).
897 <https://doi.org/10.1155/2017/1654237>

898 Treude, T., Krause, S., Maltby, J., Dale, A. W., Coffin, R., & Hamdan, L. J. (2014). Sulfate reduction and
899 methane oxidation activity below the sulfate-methane transition zone in Alaskan Beaufort Sea continental
900 margin sediments: Implications for deep sulfur cycling. *Geochimica et Cosmochimica Acta*, 144, 217–
901 237. <https://doi.org/10.1016/j.gca.2014.08.018>

- 902 Treude, T., Niggemann, J., Kallmeyer, J., Wintersteller, P., Schubert, C. J., Boetius, A., & Jørgensen, B. B.
903 (2005). Anaerobic oxidation of methane and sulfate reduction along the Chilean continental margin.
904 *Geochimica et Cosmochimica Acta*, 69(11), 2767–2779. <https://doi.org/10.1016/j.gca.2005.01.002>
- 905 Valentine D. L. (2002). Biogeochemistry and microbial ecology of methane oxidation in anoxic environments:
906 A review. *Antonie van Leeuwenhoek*, 81(1-4), 271-282. <http://doi.org/10.1023/A:1020587206351>
- 907 Valenzuela, E. I., Avendaño, K. A., Balagurusamy, N., Arriaga, S., Nieto-Delgado, C., Thalasso, F., &
908 Cervantes, F. J. (2019). Electron shuttling mediated by humic substances fuels anaerobic methane
909 oxidation and carbon burial in wetland sediments. *Science of the Total Environment*, 650, 2674–2684.
910 <https://doi.org/10.1016/j.scitotenv.2018.09.388>
- 911 Valenzuela, E. I., Prieto-Davó, A., López-Lozano, N. E., Hernández-Eligio, A., Vega-Alvarado, L., Juárez, K.,
912 García-González, A. S., López, M. G., & Cervantes, F. J. (2017). Anaerobic methane oxidation driven by
913 microbial reduction of natural organic matter in a tropical wetland. *Applied and Environmental*
914 *Microbiology*, 83(11), 1–15. <https://doi.org/10.1128/AEM.00645-17>
- 915 Vigderovich, H., Liang, L., Herut, B., Wang, F., Wurgaft, E., Rubin-Blum, M., & Sivan, O. (2019). Evidence
916 for microbial iron reduction in the methanogenic sediments of the oligotrophic SE Mediterranean
917 continental shelf. *Biogeosciences Discussions*, 1–25. <https://doi.org/10.5194/bg-2019-21>
- 918 Wang, L., Miao, X., Ali, J., Lyu, T., & Pan, G. (2018). Quantification of Oxygen Nanobubbles in Particulate
919 Matters and Potential Applications in Remediation of Anaerobic Environment. *ACS Omega*, 3(9), 10624–
920 10630. <https://doi.org/10.1021/acsomega.8b00784>
- 921 Wegener G, Niemann H, Elvert M, Hinrichs K-U, Boetius A (2008). Assimilation of methane and inorganic
922 carbon by microbial communities mediating the anaerobic oxidation of methane. *Environmental*
923 *Microbiology* 10(9), 2287-2298. doi: 10.1111/j.1462-2920.2008.01653.x.
- 924 Wegener, G., Gropp, J., Taubner, H., Halevy, I., & Elvert, M. (2021). Sulfate-dependent reversibility of
925 intracellular reactions explains the opposing isotope effects in the anaerobic oxidation of methane. *Science*
926 *Advances*, 7(19), 1–14. <https://doi.org/10.1126/sciadv.abe4939>
- 927 Whiticar, M. J., Faber, E., & Schoell, M. (1986). Biogenic methane formation in marine and freshwater
928 environments: CO₂ reduction vs. acetate fermentation-Isotope evidence. *Geochimica et Cosmochimica*
929 *Acta*, 50(5), 693-709. [http://doi.org/10.1016/0016-7037\(86\)90346-7](http://doi.org/10.1016/0016-7037(86)90346-7)
- 930 Wu, Y.W., Tang, Y.-H., Tringe, S. G., Simmons, B. A., & Singer, S. W. (2014). MaxBin: an automated binning
931 method to recover individual genomes from metagenomes using. *Microbiome*, 2(26), 4904–4909.
932 Retrieved from <https://microbiomejournal.biomedcentral.com/articles/10.1186/2049-2618-2-26>
- 933 Wuebbles, D. J., & Hayhoe, K. (2002). Atmospheric methane and global change. *Earth-Science Reviews*, 57(3–
934 4), 177–210. [https://doi.org/10.1016/S0012-8252\(01\)00062-9](https://doi.org/10.1016/S0012-8252(01)00062-9)
- 935 Xu, Z., Masuda, Y., Wang, X., Ushijima, N., Shiratori, Y., Senoo, K., & Itoh, H. (2021). Genome-Based

936 Taxonomic Rearrangement of the Order Geobacterales Including the Description of *Geomonas*
937 *azotofigans* sp. nov. and *Geomonas diazotrophica* sp. nov. *Frontiers in Microbiology*, 12(September).
938 <http://doi.org/10.3389/fmicb.2021.737531>

939 Yorshansky, O. (2019). *Iron Reduction in Deep Marine Sediments of the Eastern Mediterranean Continental*
940 *Shelf and the Yarqon Estuary*. MsC thesis, Ben Gurion University of the Negev.

941 Yoshinaga, M. Y., Holler, T., Goldhammer, T., Wegener, G., Pohlman, J. W., Brunner, B., Kuypers, M. M. M.,
942 Hinrichs, K. U., & Elvert, M. (2014). Carbon isotope equilibration during sulphate-limited anaerobic
943 oxidation of methane. *Nature Geoscience*, 7(3), 190–194. <https://doi.org/10.1038/ngeo2069>

944 Zehnder, a J., & Brock, T. D. (1979). Methane formation and methane oxidation by methanogenic bacteria.
945 *Journal of Bacteriology*, 137(1), 420–432.

946 Zhang, X., Xia, J., Pu, J., Cai, C., Tyson, G. W., Yuan, Z., & Hu, S. (2019). Biochar-Mediated Anaerobic
947 Oxidation of Methane. *Environmental Science and Technology*, 53(12), 6660–6668.
948 <https://doi.org/10.1021/acs.est.9b01345>

949 Zheng, Y., Wang, H., Liu, Y., Zhu, B., Li, J., Yang, Y., Qin, W., Chen, L., Wu, X., Chistoserdova, L., & Zhao,
950 F. (2020). Methane-Dependent Mineral Reduction by Aerobic Methanotrophs under Hypoxia.
951 *Environmental Science and Technology Letters*, 7(8), 606–612. <https://doi.org/10.1021/acs.estlett.0c00436>

952